Rationalizing the Equilibration and Cooling Stages of Cryopreservation: The Effect of Cell Size Distribution

S. Fadda and A. Cincotti
Dipartimento di Ingegneria Chimica e Materiali, Università degli Studi di Cagliari, Piazza d'Armi, Cagliari 09123, Italy

G. Cao
Dipartimento di Ingegneria Chimica e Materiali, Università degli Studi di Cagliari, Piazza d'Armi, Cagliari 09123, Italy

CRS4 (Center for Advanced Studies, Research and Development in Sardinia), Località Piscinamanna, Edificio 1, Pula 09010, Cagliari, Italy

DOI 10.1002/aic.12320
Published online July 20, 2010 in Wiley Online Library (wileyonlinelibrary.com).

A novel model able to quantitatively describe intracellular ice formation (IIF) as a function of temperature in a cell population characterized by a size distribution is proposed for the case when a permeant cryoprotectant agent (CPA) is present. As such, the model represents the ideal extension of the one recently proposed by the authors for interpreting the behavior of a size-distributed population of cells during cryopreservation without CPA. To resemble the experimental procedure actually adopted, the former model is coherently modified for the simulation of the initial equilibration stage (i.e., a one-step CPA permeation kinetics into cells initially under isotonic conditions to be suspended in a water/salt/CPA solution at ambient temperature) and of the subsequent cooling stage at constant rate down to −60°C. Specifically, the size distribution dynamics of a cell population in response to water osmosis, CPA permeation, and IIF is simulated by means of a suitable population balance approach. Water and CPA intracellular transport equations based on the classical Kedem and Katchalsky formalism are coupled to the quantitative description of nucleation and diffusion-limited growth of ice crystals in the framework of a one-dimensional population balance equation. The driving forces of all the physico-chemical phenomena involved are evaluated by taking into account the relevant ternary phase diagram, whereas the viscosity of the cytoplasm solution is properly accounted as a function of the salt and CPA concentrations. After a reasoned choice of the values of model parameters, the behavior of isolated rat hepatocytes suspended in a water/sodium-chloride/glycerol solution is simulated and analyzed at different, practicable (i.e., low) constant cooling rates and CPA equilibration concentrations. It is confirmed that differently sized cells in a single population exhibit different IIF temperatures under the same operative conditions even

Correspondence concerning this article should be addressed to A. Cincotti at cincotti@dicm.unica.it or G. Cao at cao@visnu.dicm.unica.it.

in the presence of CPA. Correspondingly, the probability of IIF results to be a function of the initial size distribution of the cell population. Depending on the specific operative conditions adopted, the size distribution and the osmotic properties of the cell lineage at hand, IIF at −60°C may be lethal for a fraction of the cell population (i.e., larger size classes), or it may not reach a dangerous level for the intermediate size class cells, while it will not even take place for the smaller ones. Finally, even if no comparison with experimental data is provided, an original and physically sound explanation for several, well-known experimental evidences, which appeared in a number of articles available in the literature of cell cryopreservation with CPA, is comprehensively given. © 2010 American Institute of Chemical Engineers *AIChE J,* 57: 1075–1095, 2011
Keywords: cell number density distribution, population balance, intracellular ice formation, membrane permeability

Introduction

In the field of tissue engineering, cryopreservation of biological cells represents a current evolving technology where significant advances have been made to date, although several challenges remain.[1] Cryopreservation of suspending cells involves cooling to subzero temperatures with or without cryoprotectant agents (CPAs), storage, thawing, and return to physiological environment for specific usages. During freezing, the ice, initially formed in the extracellular medium surrounding the cells, may nucleate and grow in the cytoplasm, whereas cell volumes and intracellular composition may vary according to osmosis phenomenon. Serious damage and injury and even lethality occur during freezing due to intracellular ice formation (IIF) and ''solution effect'', i.e., membrane rupture, mechanical deformation, excessive cell dehydration, cytotoxicity, etc., taking place at high and low cooling rates and CPA concentration levels.[2,3] These phenomena may dramatically reduce cell viability after the cryopreservation cycle.

The development of cryopreservation protocols that guarantee cell survival is based,[4] from one side, on the use of effective CPAs, since the accidental discovery of glycerol[5] which is able to enhance post-thaw viability. From the other side, successful cryopreservation protocols may be established by taking advantage of suitable mathematical models, which is able to predict the behavior of cells during freezing, along the lines of the pioneering Mazur's work.[6] Indeed, because of the wide spectrum of operative conditions adopted along with the variability of the osmotic properties between different cell lineages, the extensive trial-and-error experimental campaigns necessary to find out the optimum conditions[1] need to be avoided.

Basically, suitable mathematical models have been developed in the literature to address important stages of typical cryopreservation protocol separately. In particular, Refs.[7–13] address only the osmotic behavior during equilibration without analyzing the freezing phase. Here, the aim is to determine the osmotic parameters through direct comparison with experimental data. Specifically, when CPA is used, the equilibration is modeled through the classical Kedem and Katchalsky formalism, i.e., by considering the permeation of water and CPA through cell membrane as coupled phenomena. On the other hand, Refs. [14–19] take into account only the simulation of IIF with the goal of evaluating the ice nucleation and growth parameters. Here, only water osmosis during freezing is taken into account by means of the Mazur's equation.[6] Intriguingly, the latter one is however adopted even in the presence of CPA, by taking the cell volume, when freezing starts, equal to the isotonic one, regardless of the CPA concentration used. In this case, the modeling of the equilibration phase is circumvented by simply replacing some of the intracellular water with the exact amount of CPA necessary to obtain an equal value of its internal and external concentrations, while IIF is either accounted for as taking place within a single representative (i.e., average) cell[17] or the probability of IIF (PIIF) is related to the nucleation rate by assuming sporadic nucleation of identical cells.[15]

Recently, a novel model based on population balance equations (PBEs) approach is proposed to quantitatively interpret the behavior of a population of biological cells during the cooling stage of a cryopreservation procedure in the absence of CPA.[20] Specifically, the natural size distribution of a population of cells of the same lineage was invoked to interpret the experimental evidence that IIF takes place at different temperatures, depending on the specific operative conditions adopted. It was found that IIF temperature depends on the cell size, i.e., it is higher for larger cells, and, correspondingly, the PIIF results to be dependent on the initial size distribution of the cell population.

In this work, this original perspective is extended to the case when CPA is present, as this aspect was not previously considered. The model aims to simulate the initial equilibration stage of a population of spherical biological cells characterized by a certain size distribution suspended in a water/salt/CPA solution at ambient temperature (i.e., when intracellular CPA permeation occurs), and the subsequent cooling stage at constant rate down to −60°C. These are two steps actually performed during standard experimental procedures of cell cryopreservation with CPA. Size distribution dynamics of a cell population in response to water osmosis, CPA permeation, and IIF are simulated by means of a suitable PBEs approach. From this point of view, we bridge the gap between the two models of cryopreservation stages proposed so far in the literature and briefly described above, as the quantitative description of nucleation and diffusion-limited growth of ice crystals inside any size class of the cell population is coupled to water and CPA intracellular transport equations based on the Kedem and Katchalsky formalism.

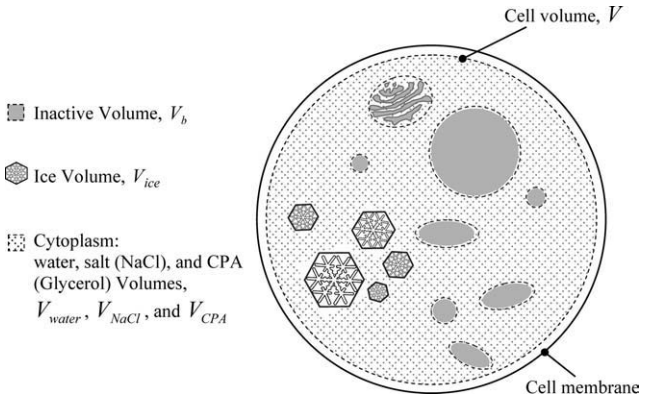

Figure 1. Schematic representation of the cell model.

Model Equations

The proposed model aims to simulate the initial equilibration stage of a population of spherical biological cells characterized by a certain size distribution suspended in a water/salt/CPA solution at ambient temperature (i.e., intracellular CPA permeation), and the subsequent cooling stage at constant rate down to $-60°C$.

Each cell is represented as surrounded by a semipermeable membrane, as depicted in Figure 1. Proteins, organelles, and other macromolecules are representatives of the cell volume V_b that remains inactive to all physical processes considered in the proposed model. On the other hand, total cell volume V changes due to water osmosis and CPA permeation that occur during equilibration and freezing, where intracellular ice crystal nucleation and growth also take place. Water osmosis, CPA permeation, and IIF determine the corresponding variation of intracellular salt and CPA concentrations and, thus, of water, ice, and CPA volumes, i.e., V_{water}, V_{ice}, and V_{CPA}, respectively.

The model is based on the following assumptions:

- The capacity of the extracellular solution is much higher than the cumulative cytoplasm capacity of the suspended cell population.
- During the cooling stage, the extracellular solution and ice formed are under thermodynamic equilibrium conditions at each temperature level reached according to the relevant ternary phase diagram.
- Space intracellular and extracellular temperature gradients are neglected, i.e., temperature is homogenously distributed throughout the system.
- Intracellular and extracellular aqueous solutions are considered ideal and dilute.
- Constant densities.
- Negligible difference between ice and liquid water densities.
- Constant osmotically inactive cell volume fraction, V_b.
- Negligible impingement between intracellular ice crystals.

In particular, the first four simplifying assumptions deserve a comment/justification. Basically, it is reasonable that the capacities of the two compartments (extracellular and intracellular) involved in water osmosis and CPA permeation are very much different when considering the typical operative conditions actually adopted during cryopreservation (i.e., one million of cells with an average diameter of 10 μm with a maximum total cytoplasmic volume of 5.2×10^{-4} ml suspended in about 1 ml aqueous solution). As a consequence, water osmosis and CPA permeation cannot significantly change extracellular solution composition and volume, which are thus modeled as constants with time during equilibration stage at ambient temperature. The assumption that extracellular solution is under thermodynamic equilibrium conditions, with the extracellular ice formed at each temperature level reached is related to the same aspect. Indeed, due to the relatively higher capacity of extracellular solution, ice formation is faster with respect to the intracellular one.[21,22] In fact, according to the classical nucleation theory, the ice nucleation rate increases if water volume increases due to the statistically more frequent nucleation impact between water molecules. Therefore, for the sake of model simplicity, it is implicitly assumed that the time scale of nucleation is much smaller in the extracellular solution than inside the cells, and, accordingly, the corresponding ice formation dynamics is so fast to practically reach equilibrium condition instantaneously.

Regarding the assumption of the absence of spatial temperature gradients inside the modeled system, it seems reasonable that only negligible temperature differences may develop locally between each cell and the surrounding aqueous medium as a consequence of the involved length scales. However, as no stirring of the liquid extracellular solution is actually performed during a standard cryopreservation protocol, it is likely that spatial temperature gradients develop inside the system, depending on the relative distance from the walls of the vessel containing the modeled suspension and the adopted operative conditions. On the other hand, the controlled rate freezers and vessels currently used for the kind of experiments simulated in this work possess relative sizes that allow to reasonably assume negligible temperature gradients. Indeed, usually thin straws (0.25 ml) or small vials (1–2 ml) are the standard vessels containing the suspension that is typically adopted, to be inserted inside a relatively large capacity cooling chamber (1–400 l).

Finally, the assumption that aqueous solutions for intracellular and extracellular compartments are ideal and dilute implies that the driving forces appearing in the proposed model are determined by using concentrations expressed in terms of osmolality, according to the Kedem and Katchalsky formalism for osmotic rates, as reported in Ref. 23. Indeed, for a dilute solution, osmolality is equal to molality for undissociated species, while it is expressed as the product between molality and the dissociation constant for salts like sodium chloride (NaCl). On the other hand, very high concentrated solutions may be reached during a cryopreservation protocol. Thus, the assumption of ideal and dilute solution does not represent the actual system behavior, although it is widely used in the literature. It is worth noting that, even if the general, qualitative results on system behavior interpretation obtained through the model proposed in this work do not change, the assumption of ideal and dilute solutions should be removed when aiming to a quantitative agreement with experimental data. Specifically, to correlate osmolality and molality at high concentrations, the osmotic virial equation suggested in Ref. 24 may be taken into account.

Model equations along with the corresponding initial and boundary conditions are summarized in Table 1. To limit the

Table 1. Model Equations

Temperature dynamics: equilibration and cooling

$$T(t) = \begin{cases} T_{\text{init}} & 0 \le t < t_{\text{eq}} \\ T_{\text{init}} - B \cdot \left(t - t_{\text{eq}}\right) & t \ge t_{\text{eq}} \end{cases} \tag{1}$$

Cell population volumic distribution dynamics

$$\frac{\partial\, n(V,t)}{\partial t} + \frac{\partial [G_v(V) \cdot n(V,t)]}{\partial V} = 0 \quad \begin{cases} n(V,t) = n^0(V) & \text{at} \quad t = 0 \quad ; \quad \forall V \in [0, +\infty[\\ \int_0^{+\infty} n(V,t)\, dV = N^0_{\text{tot}} & \forall t \end{cases} \tag{2}$$

Osmotic water and CPA transport dynamics

$$T_e \le T(t) \le T_{\text{init}} \text{ (Equilibration and cooling down to entectic temperature)}$$

$$\frac{dV}{dt} = G_v(V) = \frac{d(V_{\text{water}} + V_{\text{CPA}})}{dt} = -L_p(t) \cdot A(t) \cdot \Re \cdot T(t) \left[\left(M^{\text{ext}}_{\text{NaCl}}(t) - M^{\text{int}}_{\text{NaCl}}(t)\right) + \sigma \left(M^{\text{ext}}_{\text{CPA}}(t) - M^{\text{int}}_{\text{CPA}}(t)\right)\right];\ V = V_0 \text{ at } t = 0 \tag{3}$$

$$\frac{dn_{\text{CPA}}}{dt} = (1-\sigma) \cdot \left(\frac{M^{\text{ext}}_{\text{CPA}}(t) + M^{\text{int}}_{\text{CPA}}(t)}{2}\right) \frac{dV}{dt} + P_{\text{CPA}}(t) \cdot A(t) \cdot \left(M^{\text{ext}}_{\text{CPA}}(t) - M^{\text{int}}_{\text{CPA}}(t)\right); \quad n_{\text{CPA}} = 0 \quad \text{at} \quad t = 0 \tag{4}$$

$$M^{\text{int}}_{\text{NaCl}}(t) = \frac{\varphi\, n_{\text{NaCl}}}{V_{\text{water}}(t)} \tag{5}$$

$$M^{\text{int}}_{\text{CPA}}(t) = \frac{n_{\text{CPA}}(t)}{V_{\text{water}}(t)} \tag{6}$$

$$\left.\begin{array}{l} M^{\text{ext}}_{\text{NaCl}}(t) = M^{\text{ext}}_{\text{NaCl},0} \\ M^{\text{ext}}_{\text{CPA}}(t) = M^{\text{ext}}_{\text{CPA},0} \end{array}\right\} \quad \textit{if} \quad T_f \le T(t) \le T_{\text{init}} \tag{7}$$

(8)

$$\left.\begin{array}{l} M^{\text{ext}}_{\text{NaCl}}(t) = M^{\text{eq,ext}}_{\text{NaCl}}(t) = \frac{1}{\nu_{H_2O}} \frac{S^{\text{ext}}_{\text{eq}}(t)}{\left(100 - S^{\text{ext}}_{\text{eq}}(t)\right)} \cdot \frac{\varphi}{(R^{\text{ext}}+1)} \cdot \frac{MW_{H_2O}}{MW_{\text{NaCl}}} \\ M^{\text{ext}}_{\text{CPA}}(t) = M^{\text{eq,ext}}_{\text{CPA}}(t) = \frac{1}{\nu_{H_2O}} \frac{S^{\text{ext}}_{\text{eq}}(t)}{\left(100 - S^{\text{ext}}_{\text{eq}}(t)\right)} \cdot \frac{R^{\text{ext}}}{(R^{\text{ext}}+1)} \cdot \frac{MW_{H_2O}}{MW_{\text{CPA}}} \end{array}\right\} \quad \textit{if} \quad T_e \le T(t) < T_f \tag{9}$$

(10)

$$R^{\text{ext}} = \varphi \frac{MW_{\text{CPA}}}{MW_{\text{NaCl}}} \frac{M^{\text{ext}}_{\text{CPA},0}}{M^{\text{ext}}_{\text{NaCl},0}} \tag{11}$$

$$S^{\text{ext}} = 100 \cdot \frac{\frac{MW_{\text{NaCl}}}{\varphi} \cdot M^{\text{ext}}_{\text{NaCl},0} + MW_{\text{CPA}} \cdot M^{\text{ext}}_{\text{CPA},0}}{\frac{MW_{\text{NaCl}}}{\varphi} \cdot M^{\text{ext}}_{\text{NaCl},0} + MW_{\text{CPA}} \cdot M^{\text{ext}}_{\text{CPA},0} + \frac{MW_{H_2O}}{\nu_{H_2O}}} \quad \text{if} \quad T_f \le T(t) \le T_{\text{init}} \tag{12}$$

$$S^{\text{ext}} = S^{\text{ext}}_{\text{eq}} = f(R^{\text{ext}}, T) \quad \text{through Eq. (19)} \qquad \text{if} \quad T_e \le T(t) < T_f \tag{13}$$

$$L_p(t) = L_{p,\text{ref}} \cdot \exp\left(-\frac{E_w}{\Re}\left(\frac{1}{T(t)} - \frac{1}{T_{\text{ref}}}\right)\right) \tag{14}$$

$$P_{\text{CPA}}(t) = P_{\text{CPA,ref}} \cdot \exp\left(-\frac{E_{\text{CPA}}}{\Re}\left(\frac{1}{T(t)} - \frac{1}{T_{\text{ref}}}\right)\right) \tag{15}$$

$$A(t) = 4\pi \cdot \left(\frac{3}{4\pi}\right)^{2/3} \cdot V(t)^{2/3} \tag{16}$$

Table 1. Continued

$T(t) < T_e$ (Cooling below eutectic temperature)

$$\frac{dV}{dt} = G_v(V) = \frac{d(V_{water} + V_{CPA})}{dt} = 0; \tag{17}$$

$$\frac{dn_{CPA}}{dt} = 0 \tag{18}$$

Ternary phase diagram (H_2O/NaCl/glycerol) - Liquidus surface and eutectic temperature

$$T(R, S_{eq}) = \alpha \cdot S_{eq}(t) + \beta \cdot S_{eq}(t)^2 \qquad \begin{cases} \alpha = \frac{1}{-1.6 - 1.27 \cdot R(t) - 0.25 \cdot R(t)^2} \\ \beta = -0.01 \end{cases} \tag{19}$$

$$T_e = \begin{cases} 251.8 - 4.55 \cdot R^{ext} - 0.55 \cdot R^{ext^2} & \text{if } 0 \le R^{ext} \le 7 \\ 226.5 - \frac{234.4}{R^{ext}} & \text{if } R^{ext} > 7 \end{cases} \tag{20}$$

Intracellular liquid water volume

$$V_{water}(t) = V(t) - V_b - V_{NaCl} - V_{CPA}(t) - V_{ice}(t) \tag{21}$$

$$V_b = v_b \cdot V_0 \tag{22}$$

$$V_{NaCl} = v_{NaCl} \cdot n_{NaCl} = v_{NaCl} \cdot c_0 \cdot (1 - v_b) \cdot V_0 \tag{23}$$

$$V_{CPA}(t) = v_{CPA} \cdot n_{CPA}(t) \tag{24}$$

Intracellular Ice Mass Balance

$$V_{ice}(t) = \begin{cases} 0 & \text{if} \quad N_{ice}(t) = 0 \\ \sum_{i=1}^{N_{ice}(t)} \frac{4\pi}{3} [r_i(t)]^3 & \text{if} \quad N_{ice}(t) \ge 1 \end{cases} \tag{25}$$

$$N_{ice}(t) = \text{int}\left(\overline{N}_{ice}(t)\right) \tag{26}$$

Nucleation and growth of Intracellular Ice Crystals

$$\frac{d\bar{N}_{ice}}{dt} = \begin{cases} 0 \quad ; \quad \bar{N}_{ice} = 0 \quad \text{at} \quad t = 0 \quad \text{if} \quad T_f \le T(t) \le T_{init} \\ B_0(t) \quad ; \quad \bar{N}_{ice} = 0 \quad \text{at} \quad t = 0 \quad \text{if} \quad T(t) < T_f \end{cases} \tag{27}$$

$$B_0(t) = J(t) \cdot (V(t) - V_b - V_{ice}(t)) \tag{28}$$

$$J(t) = J_0 \cdot D(t) \cdot \exp\left(-\frac{E_N(t)}{k_B \cdot T(t)}\right) \tag{29}$$

$$E_N(t) = \frac{4}{3}\pi \cdot \gamma \cdot [r^*(t)]^2 \tag{30}$$

$$r^*(t) = \frac{2 \cdot \gamma}{\Re \cdot T(t) \cdot \left[\left(M_{NaCl}^{eq,int}(t) - M_{NaCl}^{int}(t)\right) + \left(M_{CPA}^{eq,int}(t) - M_{CPA}^{int}(t)\right)\right]} \tag{31}$$

$$M_{NaCl}^{eq,int}(t) = \frac{1}{v_{H_2O}} \frac{S_{eq}^{int}(t)}{\left(100 - S_{eq}^{int}(t)\right)} \cdot \frac{\varphi}{(R^{int}(t) + 1)} \cdot \frac{MW_{H_2O}}{MW_{NaCl}} \tag{32}$$

Table 1. Continued

$$M_{\mathrm{CPA}}^{\mathrm{eq,int}}(t)=\frac{1}{v_{\mathrm{H_2O}}}\frac{S_{\mathrm{eq}}^{\mathrm{int}}(t)}{\left(100-S_{\mathrm{eq}}^{\mathrm{int}}(t)\right)}\cdot\frac{R^{\mathrm{int}}(t)}{\left(R^{\mathrm{int}}(t)+1\right)}\cdot\frac{MW_{\mathrm{H_2O}}}{MW_{\mathrm{CPA}}} \tag{33}$$

$$R^{\mathrm{int}}(t)=\varphi\frac{MW_{\mathrm{CPA}}}{MW_{\mathrm{NaCl}}}\frac{M_{\mathrm{CPA}}^{\mathrm{int}}(t)}{M_{\mathrm{NaCl}}^{\mathrm{int}}(t)} \tag{34}$$

$$D(t)=\frac{k_{\mathrm{B}}\cdot T(t)}{6\pi\cdot a_0\cdot\eta(t)} \tag{35}$$

$$\eta(t)=\eta_{\mathrm{CPA}}\left(M_{\mathrm{CPA}}^{\mathrm{int}},T\right)\cdot\exp\left(\frac{k_{\mathrm{e}}\cdot\phi_{\mathrm{s}}\left(M_{\mathrm{NaCl}}^{\mathrm{int}},M_{\mathrm{CPA}}^{\mathrm{int}}\right)}{1-Q\cdot\phi_{\mathrm{s}}\left(M_{\mathrm{NaCl}}^{\mathrm{int}},M_{\mathrm{CPA}}^{\mathrm{int}}\right)}\right) \tag{36}$$

$$\eta_{\mathrm{CPA}}\left(M_{\mathrm{CPA}}^{\mathrm{int}},T\right)=A_{\mathrm{CPA}}\left(M_{\mathrm{CPA}}^{\mathrm{int}}\right)\cdot\exp\left(\frac{E_{\eta_{\mathrm{CPA}}}\left(M_{\mathrm{CPA}}^{\mathrm{int}}\right)}{T(t)-T_{\mathrm{c}}\left(M_{\mathrm{CPA}}^{\mathrm{int}}\right)}\right) \tag{37}$$

$$\phi_{\mathrm{s}}\left(M_{\mathrm{NaCl}}^{\mathrm{int}},M_{\mathrm{CPA}}^{\mathrm{int}}\right)=\frac{\left(v_{\mathrm{NaCl}}+h\cdot v_{\mathrm{H_2O}}\right)\cdot M_{\mathrm{NaCl}}^{\mathrm{int}}(t)}{\varphi+\varphi\cdot v_{\mathrm{CPA}}\cdot M_{\mathrm{CPA}}^{\mathrm{int}}(t)+v_{\mathrm{NaCl}}\cdot M_{\mathrm{NaCl}}^{\mathrm{int}}(t)} \tag{38}$$

$$A_{\mathrm{CPA}}\left(M_{\mathrm{CPA}}^{\mathrm{int}}\right)=\eta_{\mathrm{CPA}}^{T_{\mathrm{g}}}\cdot\exp\left[-\frac{E_{\eta_{\mathrm{CPA}}}\left(M_{\mathrm{CPA}}^{\mathrm{int}}\right)}{T_{\mathrm{g}}\left(M_{\mathrm{CPA}}^{\mathrm{int}}\right)-T_{\mathrm{c}}\left(M_{\mathrm{CPA}}^{\mathrm{int}}\right)}\right] \tag{39}$$

$$E_{\eta_{\mathrm{CPA}}}\left(M_{\mathrm{CPA}}^{\mathrm{int}}\right)=\ln\left(\frac{\eta_{\mathrm{CPA}}^{T_{\mathrm{g}}}}{\eta_{\mathrm{CPA}}^{293\mathrm{K}}\left(M_{\mathrm{CPA}}^{\mathrm{int}}\right)}\right)\cdot\frac{(1-\delta)\cdot\left(293\ K-T_{\mathrm{c}}\left(M_{\mathrm{CPA}}^{\mathrm{int}}\right)\right)}{293\ K-T_{\mathrm{g}}\left(M_{\mathrm{CPA}}^{\mathrm{int}}\right)} \tag{40}$$

$$T_{\mathrm{c}}\left(M_{\mathrm{CPA}}^{\mathrm{int}}\right)=\delta\cdot T_{\mathrm{g}}\left(M_{\mathrm{CPA}}^{\mathrm{int}}\right) \tag{41}$$

$$\frac{dr_i}{dt}=\begin{cases}\text{if}\ \ T_{\mathrm{f}}\le T(t)\le T_{\mathrm{init}} & \frac{dr_i}{dt}=0;\quad r_i=0\quad\text{at}\quad t=0\\ \text{if}\ \ T(t)\le T_{\mathrm{f}} & \begin{cases}r_i(t)=0 & \text{at}\quad t<t_i\quad\text{when}\quad N_{\mathrm{ice}}(t)=0\\ \frac{dr_i}{dt}=\bar{D}(t)\cdot\frac{\Omega_{\mathrm{g}}(t)}{r_i} & ;\quad r_i(t)=r^*(t)\quad\text{at}\quad t=t_i\quad\forall i\in[1;N_{\mathrm{ice}}(t)]\end{cases}\end{cases} \tag{42}$$

$$\Omega_{\mathrm{g}}(t)=\frac{\left[\left(M_{\mathrm{NaCl}}^{\mathrm{eq,int}}(t)-M_{\mathrm{NaCl}}^{\mathrm{int}}(t)\right)+\left(M_{\mathrm{CPA}}^{\mathrm{eq,int}}(t)-M_{\mathrm{CPA}}^{\mathrm{int}}(t)\right)\right]}{\left[1+\left(\left(M_{\mathrm{NaCl}}^{\mathrm{int}}(t)+M_{\mathrm{CPA}}^{\mathrm{int}}(t)\right)\cdot v_{\mathrm{H_2O}}\right)\right]\cdot\left(\left(M_{\mathrm{NaCl}}^{\mathrm{eq,int}}(t)+M_{\mathrm{CPA}}^{\mathrm{eq,int}}(t)\right)\right)} \tag{43}$$

$$\bar{D}(t)=\frac{\left(D(t)-D_{\mathrm{eq}}(t)\right)}{\ln\left(\frac{D(t)}{D_{\mathrm{eq}}(t)}\right)} \tag{44}$$

$$\eta_{\mathrm{ice}}(t)=\frac{V_{\mathrm{ice}}(t)}{V(t)-V_{\mathrm{b}}-V_{\mathrm{CPA}}} \tag{45}$$

$$\mathrm{PIIF}(t)=\frac{\int_0^{+\infty}n(V,t)|_{\eta_{\mathrm{ice}}\ge 50\%}\,dV}{N_{\mathrm{tot}}^0} \tag{46}$$

$$\eta_{\mathrm{water}}(t)=\frac{V_{\mathrm{ice}}(t)+V_{\mathrm{water}}(t)}{V(t)} \tag{47}$$

$$\mathrm{PIIF}_{\mathrm{detect}}(t)=\frac{\int_0^{+\infty}n(V,t)|_{\substack{\eta_{\mathrm{ice}}\ge 50\%;\\ \eta_{\mathrm{water}}\ge 10\%}}\,dV}{N_{\mathrm{tot}}^0} \tag{48}$$

$$\mathrm{PIIF}_{\mathrm{init}}(t)=\frac{\int_0^{+\infty}n(V,t)|_{\eta_{\mathrm{ice}}>0}\,dV}{N_{\mathrm{tot}}^0} \tag{49}$$

article length, only the new aspects of the model related to the presence of CPA are highlighted/discussed in this section. The interested reader should refer to authors' previous work[20] for a more detailed analysis of the modeling approach and the corresponding numerical strategy adopted for its solution.

According to Table 1, the system temperature is varied with time at a constant cooling rate, B, starting from the initial value T_{init} (Eq. 1) down to $-60°C$, to take into account only heterogeneous nucleation as the mechanism responsible for IIF. Actually, it is generally accepted that, in a pure water system the homogeneous nucleation starts at about $-40°C$, which represents a limit that decreases when aqueous solutions with increasing content of solutes are considered,[25] as in the system addressed in this work. Thus, the choice to limit temperature decrease down to $-60°C$ to avoid the simulation of homogenous nucleation as a simultaneous mechanism for IIF may not be completely justified. This is especially true at high cooling rates, when a hindered water exo-osmosis prevents the increase of intracellular content of solute, so that a relatively higher temperature limit for homogenous nucleation results. However, as very recently reported in Ref. 19, at relatively low freezing rates, heterogeneous nucleation should represent the only mechanism of IIF before reaching $-60°C$. According to this picture, it is worth noting that once heterogeneous nucleation starts, thus consuming intracellular liquid water to form ice, homogeneous nucleation should not take place, due to the small volume of residual water inside the icing-up cells.

The dynamics of the cell population volumic distribution during the cryopreservation protocol is quantitatively described by means of the one-dimensional PBE reported in Eq. 2, along with the corresponding initial and boundary conditions. In particular, the mathematical description of water osmosis and CPA permeation is based on Kedem and Katchalsky formalism,[26] which permits to determine the growth rate [$G_v(V)$ in Eq. 3] and the cytoplasmic content (n_{CPA} in Eq. 4) in each size class of the cell population as driven by the corresponding gradients between intracellular and extracellular solutes concentrations (M), i.e., Eqs. 5–6 and 7–10, respectively. Ideal and dilute liquid solutions are considered in the model, as clearly indicated by the linear driving forces appearing in Eqs. 3, 4, 29, and 41, while the classic Arrhenius-like temperature dependence[27] for the membrane permeabilities to water and CPA, i.e., L_p and P_{CPA}, respectively, is taken into account by Eqs. 12 and 13.

According to the simplifying assumptions discussed above, during equilibration and cooling down to melting temperature (T_f), the extracellular osmolarities of solutes (M^{ext}_{NaCl} and M^{ext}_{CPA}) do not change with time (Eqs. 7 and 8), while at lower temperatures, the aqueous solution in the extracellular compartment is assumed to be at equilibrium conditions with the corresponding ice (Eqs. 9 and 10). In particular, the ternary phase diagram of water/NaCl/glycerol available in the literature[28] is considered in this work. As reported by Eq. 17, the liquidus surface of this ternary phase diagram results to be a function of temperature (T), mass ratio between CPA and salt content (R), and total solutes wt % (S). Thus, while a constant solutes mass ratio is considered for the extracellular solution during equilibration and cooling (R^{ext} in Eq. 11), the total solute wt % (S^{ext}) is evaluated differently if system temperature is higher or lower than melting temperature (T_f). If $T \geq T_f$, the total solute wt % of the extracellular solution is constant as determined by the adopted operative conditions (see Eq. 12), and the melting point temperature T_f can be explicitly evaluated from Eq. 19 as $T_f = T(R^{ext}, S^{ext})$. On the contrary, when $T < T_f$, Eq. 19 is used to implicitly calculate the total solute wt % in the extracellular compartment under thermodynamic equilibrium condition, S^{ext}_{eq}, using the system temperature T (given by Eq. 1) and R^{ext} (given by Eq. 11). The obtained value is used to determine the extracellular osmolarities of solutes, M^{ext}_{NaCl} and M^{ext}_{CPA} through Eqs. 9 and 10. It is worth noting that, at temperatures lower than eutectic point (T_e, Eq. 20), water osmosis and CPA permeation vanish (Eqs. 17 and 18) as the liquid phase is no longer present in the extracellular medium, according to the system phase diagram.

The intracellular liquid water volume, V_{water}, used to evaluate intracellular solutes concentrations (Eqs. 5 and 6) may be obtained through Eq. 21, where all the contributions to cell volume V, as depicted in Figure 1, are taken into account (Eqs. 22–25). It should be noted that, the CPA volume is evaluated by accounting the number of CPA moles (n_{CPA}) dissolved in the intracellular solution (Eq. 24), as calculated through Eq. 4.

According to our previous work,[20] the intracellular ice volume V_{ice}, appearing in Eq. 21, for any size class cell of the considered population is determined through a discrete modeling approach, by following the fate of any single ice nucleus that is first formed and then grows as time increases (Eq. 25 and 26). Actually, the use of a PBE continuous modeling approach has been attempted for simulating ice nucleation and growth inside any size class of the cell population. However, due to the operative conditions considered in this work (i.e., low cooling rates and CPA concentrations) and the assumption that only heterogeneous nucleation occurs even in the presence of CPA, the internal ice nucleation takes place at relatively high temperatures, i.e., when crystal growth is relatively fast. Therefore, the rapid ice crystal growth along with a small control volume (i.e., cell volume) generates only a very limited number of ice crystals inside any single size class cell of the population. Consequently, the adoption of a PBE modeling approach for IIF simulation is not appropriate.

The discrete model adopted for describing ice nucleation (Eqs. 27–31) and growth (Eqs. 42–44) is the same as the one adopted in authors' previous article,[20] except for the evaluation of the driving forces appearing in Eqs. 31 and 43, where both salt and CPA content are taken into account. As intracellular solutes concentrations are generally different from the extracellular ones, the corresponding equilibrium concentrations ($M^{eq,int}_{NaCl}$ and $M^{eq,int}_{CPA}$), required to evaluate the driving forces of IIF, need to be obtained for any size class of the cell population. Thus, based on Eqs. 5 and 6, intracellular solutes concentrations are used to determine the intracellular mass ratio between CPA and salt content (R^{int}, Eq. 34). The latter one, along with the system temperature provided by Eq. 1, is used to implicitly calculate the intracellular solutes wt % at equilibrium (S^{int}_{eq}) appearing in Eqs. 32 and 33. Analogous to authors' previous model,[20] intracellular solution diffusivity (D) is estimated through the Stokes–Einstein equation (Eq. 35) based on the value of cytoplasmic viscosity η. The latter one is determined as a function of

temperature, salt, and CPA concentrations, as strongly suggested in Ref. 18. Specifically, as reported in Eq. 34, the viscosity of the ternary system is obtained by means of a mixing rule based on Vand's hard sphere model[29–31] and the solution viscosity of the binary system water/CPA (η_{CPA}, Eq. 37).

For a proper comparison between experimental data and modeling results, in addition to the ice volume fraction (η_{ice}) and PIIF (Eqs. 45 and 46) already considered in our previous article,[20] the fraction of solid and liquid water (η_{water}) inside any single size class of the cell population, and the detectable probability of internal ice formation ($PIIF_{detect}$), defined in Eqs. 47 and 48, are introduced for the first time in this work. Specifically, the iced up cells are assumed to be experimentally detectable, if the ice volume fraction reaches the value of 0.5 (i.e., $\eta_{ice} \geq 0.5$), while a relatively small content of intracellular water equal to 10 vol % is maintained (i.e., $\eta_{water} \geq 0.1$). Accordingly, the $PIIF_{detect}$ is evaluated at each temperature level as the fraction of cells with respect to the total initial ones cumulatively frozen at that temperature, while containing a preset small amount of water. The choice of a specific threshold value for η_{water} to detect ice formation is quite reasonable. Indeed, the volumic content of total water ($V_{water} + V_{ice}$) inside the cells may be relatively small with respect to CPA and inactive volumes, V_{CPA} and V_b, respectively, appearing in Eq. 21. Therefore, ice formation may not be experimentally detectable through the darkening/flashing of the cell, classically observed by means of a cryomicroscope, even if the water contained in the cell is completely turned into ice (i.e., $\eta_{ice} \rightarrow 1$ and $V_{water} \rightarrow 0$).

Alternatively, as very recently proposed in the literature,[32] IIF may be measured by means of an high-speed (8000 fps) video cryomicroscopy system. This way, cells at initial stage of ice formation (before flashing takes place) may be numbered, and a cumulative incidence of initial IIF ($PIIF_{init}$) may be experimentally determined. This new cumulative fraction of cells when icing starts to occur (i.e., when η_{ice} becomes different from zero, $\eta_{ice} > 0$) is correspondingly defined by Eq. 49 in the model proposed in this work.

Results and Discussion

The mathematical model proposed in this work is applied to quantitatively describe and predict IIF taking place in a cell population characterized by a size distribution during a cooling stage down to −60°C of a standard cryopreservation protocol with a one-step addition of a permeant CPA. Although cell cryopreservation has been modeled during the last 50 years, a complete set of parameters as well as the initial cell density distribution, the relevant ternary phase diagram, and the viscosity equation to be adopted for the solution of the proposed model are not available for any of the system investigated so far in the literature. This is mainly due to the original interpretation of IIF proposed in this work, which is based on the size distribution of the specific cell population considered, which has been completely overlooked so far in the literature. On the other hand, to describe the capabilities of the proposed theoretical approach, a model system (i.e., cells suspended in a CPA and salt aqueous solution) should be necessarily identified by properly evaluating the corresponding parameters appearing in the model equations.

Table 2. Model Parameters

Parameters	values	units	references
a_0	1.4×10^{-10}	m	33
B	1–400	°C min^{-1}	This work
c_0	142.5	mol m^{-3}	14
E_{CPA}	2.153×10^5	J mol^{-1}	This work
E_w	2.153×10^5	J mol^{-1}	20
H	1	–	20
J_0	1.748×10^{24}	# m^{-5}	20
k_e	2.5	–	14
$L_{p,ref}$	9.23×10^{-10}	m^3 N^{-1} s^{-1}	20
$M^{ext}_{CPA,0}$	0–5000	*Osmol* m^{-3}_{water}	This work
$M^{ext}_{NaCL,0}$	300	*Osmol* m^{-3}_{water}	This work
N^0_{tot}	91	–	15
$P_{CPA,ref}$	4.6×10^{-3}	m^{-1} s^{-1}	This work
Q	0.61	–	14
T_{eq}	0.03	s	This work
T_g	Figure 2a	K	34
$T_{init} = T_{ref}$	295	K	This work
φ	2	–	20
v_b	0.4937	–	20
v_{CPA}	7.3×10^{-5}	m^3 mol^{-1}	35
v_{H_2O}	1.8×10^{-5}	m^3 mol^{-1}	35
v_{NaCl}	2.69×10^{-5}	m^3 mol^{-1}	35
δ	0.885	–	36
γ	1.043×10^{-3}	J m^{-2}	20
η^{Tg}_{CPA}	10^{12}	Pa s	16
η^{273K}_{CPA}	Figure 2b	Pa s	37
σ	0.7	–	This work

Along these lines, the cryopreservation of isolated rat hepatocytes suspended in water/NaCl/glycerol solution is addressed. This choice is first related to the availability of a measured size distribution for the cell lineage considered.[15] In addition, the ternary solution of water/NaCl/glycerol is taken into account as the corresponding ternary phase diagram (Eqs. 19 and 20) and the temperature and solutes concentration dependence of viscosity are available in the literature.

The model parameters considered in this work for the system of rat hepatocytes suspended in a water/NaCl/glycerol medium solution are reported in Table 2 and Figure 2. In particular, seven of them (i.e., $L_{p,ref}$, E_w, v_b, J_o, γ, φ, and h, related to water osmosis, ice nucleation, dissociation, and hydration of NaCl) are taken from Ref. 20 by assuming that the use of CPA should not affect their corresponding values. Other parameters are available in the technical literature, as clearly indicated in Table 2. Specifically, the glass transition temperature (T_g) and the viscosity of the binary aqueous solution containing glycerol at 25°C (η^{293K}_{CPA}) as a function of CPA content (M^{int}_{CPA}) are needed to evaluate the intracellular solution viscosity through Eq. 36 in Table 1. Following Ref. 16, the experimentally determined values available in the literature[34,37] have been correlated in this work, as shown in Figures 2a, b, correspondingly.

As for the values of the remaining parameters listed in Table 2, E_{CPA} has been set equal to the activation energy of water permeability (E_w) while $P_{CPA,ref}$ has been chosen so that the corresponding ratio with the hydraulic permeability ($L_{p,ref}/P_{CPA,ref}$) falls well in the typical range (9.1×10^{-8}–6.0×10^{-7} m^2 N^{-1}) as found in the literature.[8–10] In addition, an interacting value has been assigned to the reflection coefficient σ (i.e., $\sigma < \sigma_{NI} = 0.85$), as shown in Ref. 23. The parameters B, $M^{ext}_{CPA,0}$, $M^{ext}_{NaCl,0}$, and $T_{init} = T_{ref}$ basically represent the operative conditions used during the

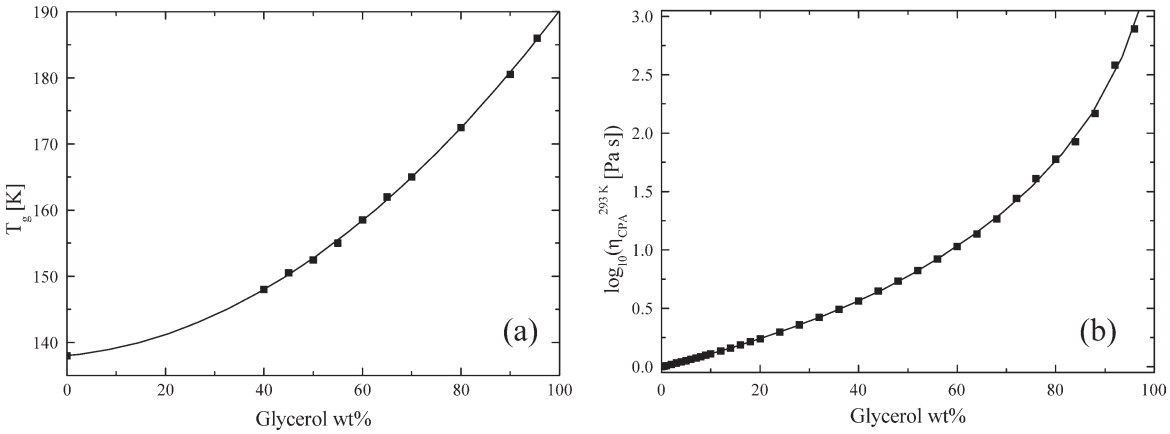

Figure 2. Glass transition temperature (a) and viscosity at 273 K (b) for the binary water–glycerol solution as a function of glycerol wt % $\left(=100\times\left[\frac{MW_{CPA}\cdot M_{CPA}}{MW_{H_2O}+MW_{CPA}\cdot M_{CPA}\cdot v_{H_2O}}\right]\right)$.

simulations. At this point, it is worth noting that only practicable operative conditions are simulated in this work, thus limiting the analysis of system behavior to the region of slow cooling rates and low CPA concentrations reported in the literature (Figure 9 in Ref. 16). Indeed, higher values of the cooling rates, i.e., 10^6–10^{13}°C/min, also considered in Ref. 16, are not usually achieved regardless the CPA concentration levels. These extreme conditions do not resemble the standard cryopreservation protocols adopted for biological samples of suspended cells and may not be obtained easily from a technological point of view. As a consequence, the simulation of system behavior under these cooling rates has not been performed, even if the corresponding upper values above where IIF does not take place and vitrification occurs, as simulated in Ref. 19 using the Karlsson's model, may be obtained through our model too. On the other hand, due to its well known cytotoxic character, the cases of high CPA concentrations are not considered in the present simulations of system behavior, thus avoiding to draw erroneous conclusions from the theoretical point of view as the proposed model does not even take into account this mechanism of cell lethality.

Starting with the size distribution of the cell population depicted in Figure 3, as determined in our previous work[20] on the basis of experimental data taken from the literature,[15] the system behavior during the one-step equilibration phase is first considered. Specifically, the dynamic evolution of the size distribution of the population of initially isotonic rat hepatocytes suspended in an aqueous solution of glycerol at 5000 $osmol_{CPA}/m^3_{water}$ at ambient temperature is simulated as shown in Figure 3. As well known in the literature, the response of the cells consists of shrinkage followed by swelling, so that the corresponding size distribution moves back and forth (i.e., initially toward smaller volumes and then toward larger ones), as water and CPA move in and out through cell membrane until the driving forces are cancelled out when intracellular and extracellular concentrations of solutes become equal.

However, depending on the CPA level considered, the cell size distribution at the end of equilibration may not coincide with the initial, isotonic one, as clearly reported in Figure 3. Thus, when cooling starts, the size distribution of the cell population may be quite different from the initial, isotonic one. This aspect is highlighted in Figure 4, where the

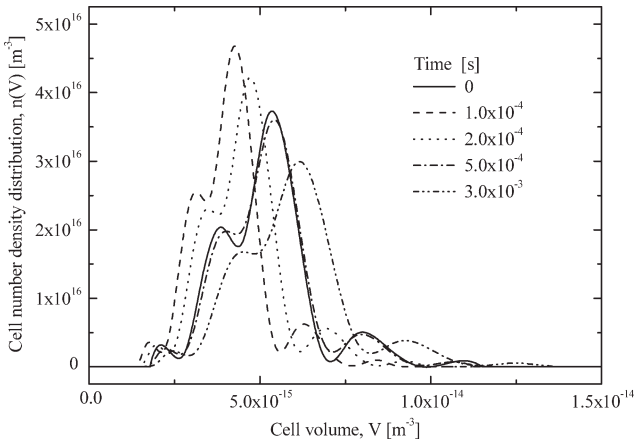

Figure 3. Model results in terms of temporal evolution of the cell number density distribution during the osmotic equilibration of cells in a 5000 Osmol m^{-3}_{water} glycerol solution.

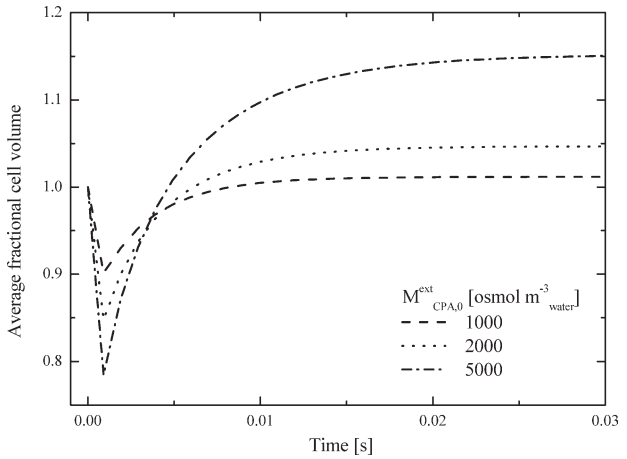

Figure 4. Model results in terms of average fractional cell volume as a function of time during equilibration at different CPA concentrations.

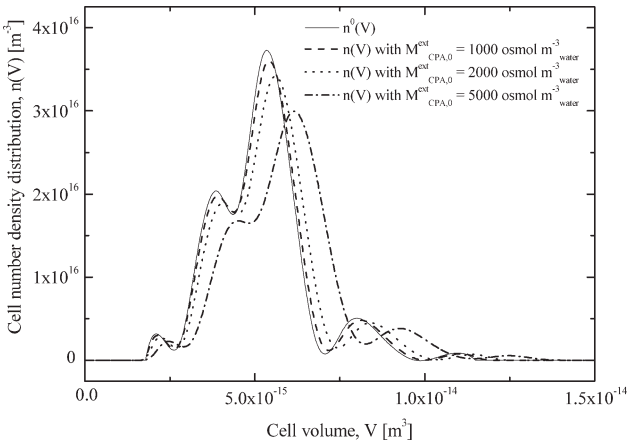

Figure 5. Cell number density distribution after equilibration in solutions of different glycerol concentrations.

temporal evolution of the average fractional cell volume of the cell population with respect to the initial one (i.e., $\frac{\int_0^\infty V \cdot n(V)\, dV}{\int_0^\infty V \cdot n^0(V)\, dV}$) is reported for the cases of glycerol addition at different concentrations, namely 1000, 2000, and 5000 $osmol_{CPA}/m^3_{water}$. The differences between initial, isotonic size distribution of the cell population and the corresponding ones at the end of the equilibration stage for different CPA concentration values may be further observed from Figure 5. Clearly, the equilibration time depends on the specific values adopted for water permeability through cell membrane. The latter one is relatively high for the rat hepatocytes (typically 30–150 s for other cell lineages[7–11,13]) due to their peculiar ability to modulate water permeability through aquaporins, necessary for carrying out their physiological task of bile secretion.[38]

However, regardless of the equilibration time, the range of cell volume variation increases with the amount of CPA used for equilibration (Figure 5). In particular, by limiting our simulations to glycerol concentrations up to 5000 $osmol_{CPA}/m^3_{water}$, the average fractional cell volume does not exceed 37% (see Figure 4). This aspect is crucial for the reliability of the simulations performed in this work. Indeed, it is well known that excessive volume excursions during pre-freezing addition and, especially, post-thawing elution of CPA may induce an osmotic stress to the cell membrane that may be lethal.[8,12,13] As this cell lethality mechanism is not taken into account in the proposed model, the CPA concentration levels used during the simulations presented in this work appear to be a proper conservative choice. This aspect represents a relevant issue. In fact, the definition of experimental protocols, where the stepwise CPA addition and elution and even the use of automated cell washers are the subjects of research articles recently published.[11,13,39,40] On the other hand, a stepwise CPA addition/removal for the reduction of cell volume variation always implies the increase of the equilibration time. Consequently, to limit longer contact times with a cytotoxic agent that may also be lethal,[41] low temperature equilibration is currently under investigation.[13,18] However, stepwise CPA addition and elution even at low temperatures represent advanced experimental protocols of cryopreservation, which are not typically adopted. Thus, the choice to simulate a one-step CPA addition phase in this work seems justified.

One of the innovative aspects of the comprehensive model proposed in this work is that the simulation of cooling stage starts from the modeling results related to the preceding equilibration stage with CPA. This novel approach permits to overcome the apparent limitation of previous IIF models related to water replacement by CPA at the end of equilibration, i.e., at the beginning of cooling stage.[16] Indeed, as it is well known by all investigators addressing the osmotic response of cells, during the one-step equilibration, CPA does not replace water, but is basically added to the cell. This may be clearly seen from Figure 6, where, by considering the largest size class cells taken as representative of the entire population, the corresponding cell volume and those ones of intracellular water and CPA [Eq. 21 in Table 1], are respectively shown after equilibration, when different extracellular CPA concentration levels are simulated. It is seen that while water volume remains constant, cell volume increases due to the CPA permeation through the membrane. As a consequence, at the end of equilibration stage (i.e., at the beginning of the cooling one) the actual intracellular water volumic content is almost similar to the initial, isotonic one, so that it remarkably affects IIF kinetics (Eqs. 21 and 28 in Table 1) and its interplay with osmosis rate. This result is in contrast with the typical consideration that IIF inhibition by CPA is partially related to the reduction of intracellular water volume through CPA entrapment during equilibration.[16,18]

Let us now turn our attention to the cooling stage of the modeled cryopreservation process. The results of the simulations in terms of PIIF as a function of temperature for different freezing rates (at various CPA concentrations) are grouped in Figure 7. A relatively complex picture of the combined effects of CPA concentration and cooling rate on PIIF is obtained. Indeed, the sigmoidal plot of PIIF reported as a function of temperature dramatically changes when varying the cooling rate. Specifically, in absence of CPA, the PIIF sigmoid moves toward higher temperatures when

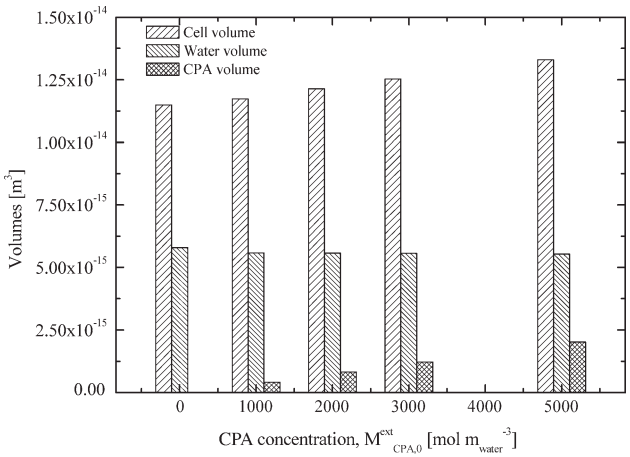

Figure 6. Histogram representing the volumic composition of the largest size class cells after equilibration with different CPA concentrations.

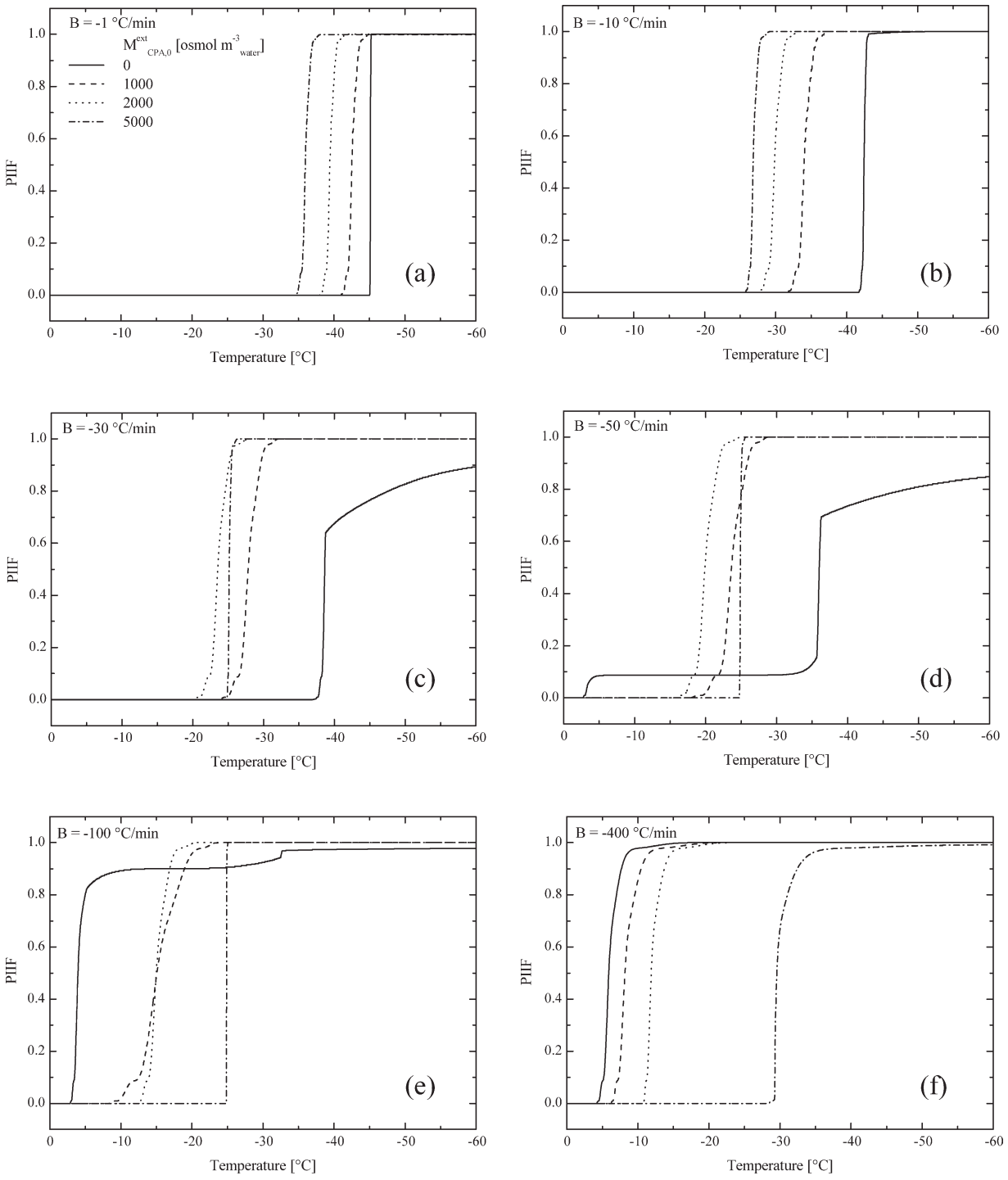

Figure 7. Model results in terms of PIIF as a function of temperature at various cooling rates and CPA concentrations.

increasing the cooling rate (cf. the solid lines of Figures 9a–d). This behavior perfectly matches with the well-known fact that cells are iced up at higher temperatures, i.e., IIF probability increases when the cooling rate is augmented. However, what is unexpected is the fact that the PIIF at -60°C shows a minimum value at intermediate cooling rates (i.e., -30 and -50°C min^{-1}, solid lines in Figures 7c, d), whereas it reaches its maximum value of 1 at the lower and higher cooling rates considered (i.e., -1 and -400°C min^{-1}, solid lines in Figures 7a–f). In other words, at intermediate cooling rates, some of the cells in the population are not iced up at -60°C, i.e., the corresponding fraction of internal ice (η_{ice}) is <50%. Moreover, at the intermediate cooling rates of -50 and -100°C min^{-1}, a two-step profile of PIIF with temperature is obtained. A qualitatively similar experimental behavior is reported in the literature.[14,42,43] Specifically, the corresponding interpretation was performed by invoking two different ice nucleation mechanisms (namely

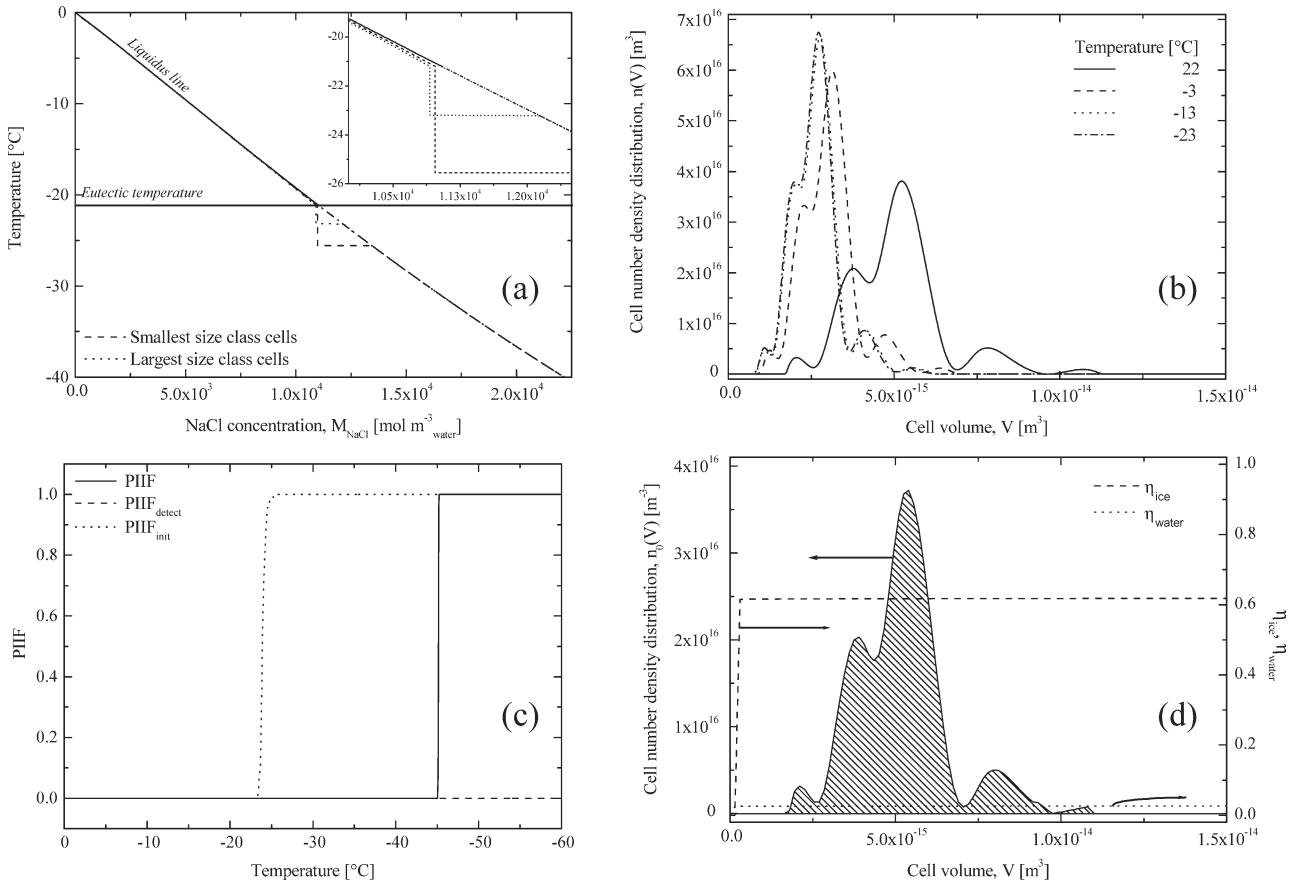

Figure 8. Model results of cooling stage of a cell suspension, carried out at -1°C min^{-1} without CPA, in terms of binary water/NaCl phase diagram with the computed NaCl concentration M_{NaCl} corresponding to the smallest (dashed line) and the largest (dotted line) size class cells (a), temporal evolution of the cell number density distribution (b), PIIF, $PIIF_{init}$, and $PIIF_{detect}$ (c), and the initial cell size, internal ice volume percentage $\eta_{ice}|_{-60°C}$, and total water content $\eta_{water}|_{-60°C}$ profiles at -60°C as a function of initial cell volume (d).

In Figure (d), cells of the initial cell size distribution that are iced up at -60°C with $\eta_{water} < 0.1$ are indicated by the light-shaded area.

surface- and volumic-catalyzed heterogeneous nucleation), acting at different temperatures on the averaged size cells, in the framework of the sporadic nucleation modeling approach. Instead, in this work, such behavior is simulated by considering only one heterogeneous nucleation mechanism of ice formation taking place in a population of differently sized cells.

It should be pointed out that these experimental data reported in the literature[14,42,43] were obtained by operating with systems and at conditions quite different from those simulated in this work. Strictly speaking, these data cannot be invoked to assess the reliability of the model proposed in this work, which can be proved on the other hand only through a specifically designed experimental campaign. However, given that comprehensive data are presently not available in the literature due to intrinsic experimental difficulties, the qualitative agreement obtained so far using our model sounds stimulating to reach an unquestionable interpretation of system behavior.

As clearly depicted in Figure 7, the effect of CPA concentration on the sigmoidal plot of PIIF vs. temperature depends on the specific cooling rate considered. In particular, such effect is not always consistent with the common knowledge that IIF temperature decrease is favored by the presence of CPA.[41,44] Indeed, at the lowest cooling rates considered (i.e., -1 and -10°C min^{-1}, see Figures 7a, b), the paradox of increasing IIF temperature when increasing CPA concentration is obtained. This undesired effect is well known in the literature.[16,41] On the contrary, a more complex behavior characterized by PIIF curves intersection when varying CPA concentration is obtained at intermediate cooling rates (i.e., -30, -50, and -100°C min^{-1}, see Figures 7c–e). Actually, consistent literature experimental data are available in terms of cumulative fraction with internal ice,[25,45] even if the corresponding theoretical interpretation was not provided as the obtained results were supposed to be the consequence of scattered measurements.

The results of the simulations reported in Figure 7 are thoroughly discussed and explained in the sequel to highlight the different roles of the physico-chemical phenomena involved during the cryopreservation of differently sized class cells of the population, by also taking advantage of some experimental evidences reported in the literature. To this aim, the case where CPA is absent is first addressed, as

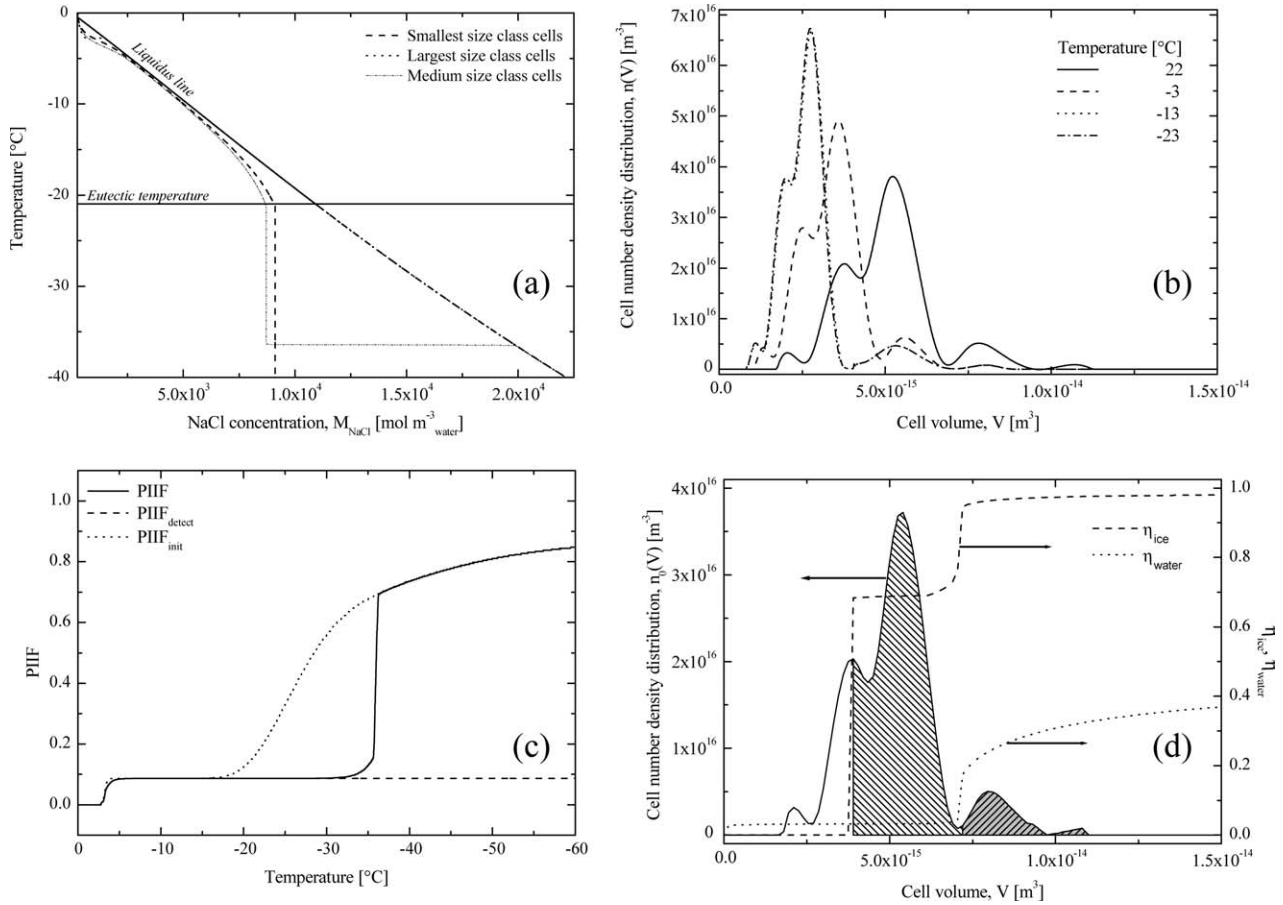

Figure 9. Model results of cooling stage of a cell suspension, carried out at $-50°C\ min^{-1}$ without CPA, in terms of binary water/NaCl phase diagram with the computed NaCl concentration M_{NaCl} corresponding to the smallest (dashed line), the largest (dotted line), and the medium- (dashed–dotted line) size class cells (a), temporal evolution of the cell number density distribution (b), PIIF, $PIIF_{init}$, and $PIIF_{detect}$ (c), and the initial cell size, internal ice volume percentage $\eta_{ice}|_{-60°C}$, and total water content $\eta_{water}|_{-60°C}$ profiles at $-60°C$ as a function of initial cell volume (d).

In Figure (d), cells of the initial cell size distribution that are iced up at $-60°C$ with $\eta_{water} \geq 0.1$, with $\eta_{water} < 0.1$ or are unfrozen, are indicated by the dark-shaded, light-shaded, or white areas, respectively.

the analysis and discussion of the behavior of a system characterized by a binary phase diagram is much simpler. It should be noted that, the initial cell size distribution will be shown during the analysis to easily discriminate the classes of cells that resulted iced up at $-60°C$ with a significant, lethal amount of intracellular water ($\eta_{ice} \geq 0.5$ and $\eta_{water} \geq 0.1$) from those iced up with a small, innocuous amount of intracellular water ($\eta_{ice} \geq 0.5$ and $\eta_{water} < 0.1$) and the unfrozen ones ($\eta_{ice} < 0.5$); the above classes are indicated by dark-shaded, light-shaded, or white areas, correspondingly.

In Figure 8, the relevant simulation results related to the cooling stage in absence of glycerol for the case of a cooling rate of $-1°C\ min^{-1}$ are reported. Basically, at relatively low cooling rates, the cells of any size class of the population are able to loose the majority of their intracellular water via osmosis, thus avoiding the undercooling at temperatures above the eutectic point ($=-21.2°C$ in this case). This is clearly depicted in Figure 8a, where the intracellular NaCl concentration M^{int}_{NaCl}, obtainable through our model, is reported on the relevant phase diagram as a function of temperature, for the smallest and the largest size class cells of the population. Since a significant water osmosis is taking place, as it may be seen from the shrinkage of the corresponding cell size distribution depicted in Figure 8b, the path of M^{int}_{NaCl} follows the liquidus line in the phase diagram of Figure 8a, until the eutectic temperature is reached. At this point, according to our model, osmosis stops and due to the consequent, unavoidable undercooling, ice begins to form inside the cells, as it may be recognized from the abrupt slope change of the corresponding path. Specifically, for the large size class cells IIF starts at relatively higher temperatures ($-23°C$) than for the small ones ($-26°C$). However, as a consequence of the significant dehydration occurred, saline concentration and viscosity of the cytoplasmic solution increases, so that ice crystals growth is very slow, as shown in Figure 8c. Here, even if the abrupt increase of $PIIF_{init}$ takes place at $-23°C$, a fraction of internal ice >50% (i.e., PIIF) is achieved only at $-45°C$. Actually, as shown in Figure 8d, for any size class cells, the highest value of η_{ice} is slightly >60% even at $-60°C$, whereas the fraction of

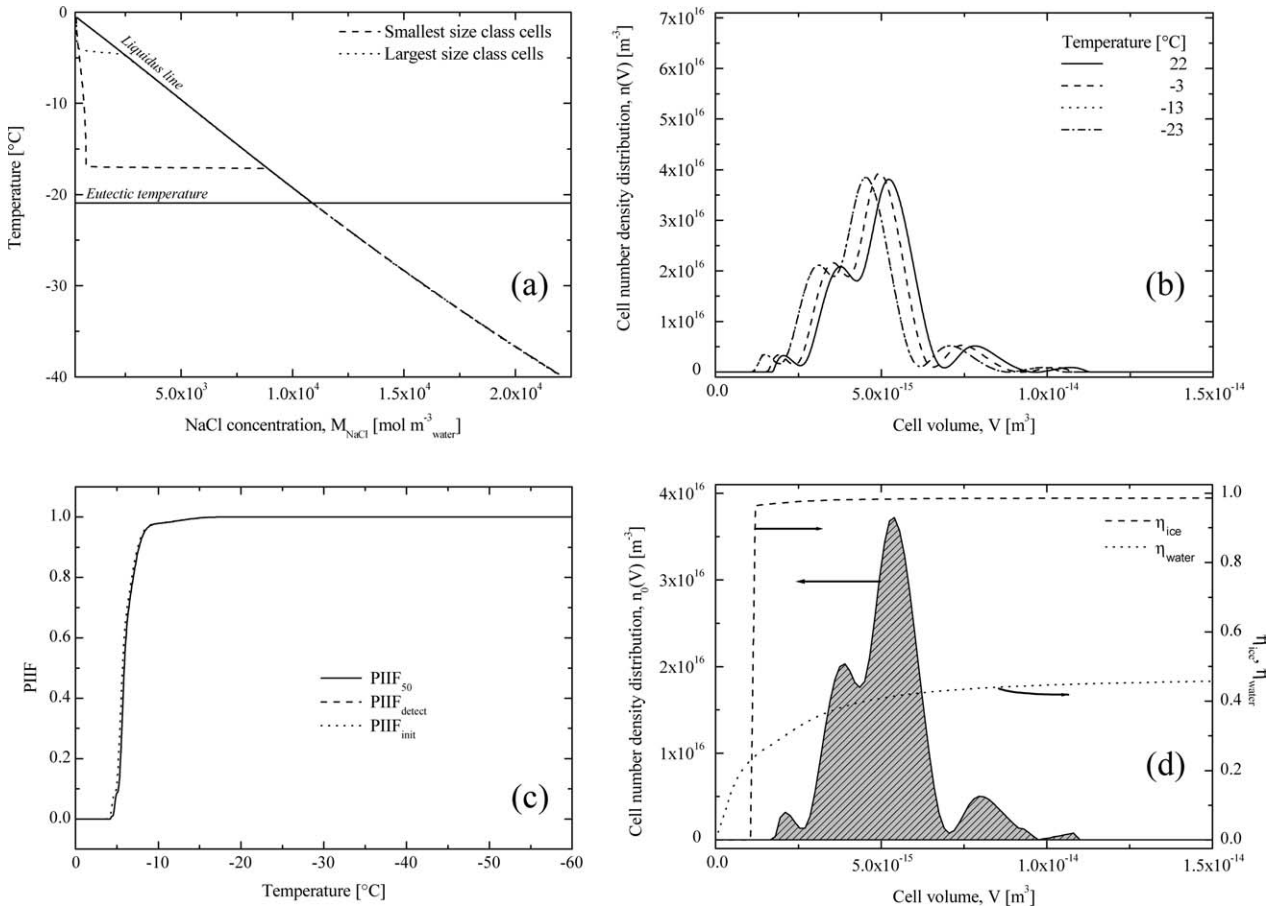

Figure 10. Model results of cooling stage of a cell suspension, carried out at -400°C min^{-1} without CPA, in terms of binary water/NaCl phase diagram with the computed NaCl concentration M_{NaCl} corresponding to the smallest (dashed line), and the largest (dotted line) size class cells (a), temporal evolution of the cell number density distribution (b), PIIF, $PIIF_{init}$, and $PIIF_{detect}$ (c), and the initial cell size, internal ice volume percentage $\eta_{ice}|_{-60°C}$, and total water content $\eta_{water}|_{-60°C}$ profiles at -60°C as a function of initial cell volume (d).

In Figure (d), cells of the initial cell size distribution that are iced up at -60°C with $\eta_{water} \geq 0.1$ are indicated by the dark-shaded area.

residual, internal water η_{water} is well below the chosen threshold of 10%. Correspondingly, the $PIIF_{detect}$ reported in Figure 8c is constantly equal to zero. Therefore, at this low cooling rate, the behavior of the cells of any size class of the population is very similar: significant dehydration, slow and only partial icing, so that a non-lethal IIF may result. On the other hand, solution injury may play a role. The same considerations are valid for the cases of -10 and -30°C min^{-1}, even if at the latter cooling rate less than 90% of the entire population of cells is iced up at -60°C (i.e., PIIF < 0.9).

The picture changes dramatically when the cooling rate is increased to -50°C min^{-1}, as shown in Figure 9. Now, the fate of the cells, as a consequence of the different interplay between osmosis and IIF, strongly depends on their initial size. Indeed, the small size class cells dehydrate significantly, so that, along with the relatively rapid decrease of temperature, the viscosity of cytoplasmic solution increases at a point that IIF does not take place even at -60°C (i.e., PIIF < 0.81 in Figure 9c). On the other hand, for the largest size class cells, osmosis is relatively slower so that undercooling and the consequent IIF take place above the eutectic temperature. In particular, these cells are responsible for the first step of PIIF reported in Figure 9c, where it is seen that a certain portion of the cell population ices up at about -4°C. At this relatively high temperature, along with a reduced water exo-osmosis that does not significantly increase the viscosity of the corresponding intracellular solution, ice growth is rapid, as it may be seen by considering the overlapping between PIIF and $PIIF_{init}$. Consistently, the entrapped and iced up intracellular water volume represents a relevant portion of these cells, so that $PIIF_{detect}$ increases to >10%, as shown in Figure 9c.

For the medium size class cells, an intermediate behavior between these two extremes occurs. The latter ones, similarly to the small size class cells, dehydrate significantly, thus following the liquidus line in Figure 9c without forming internal ice until the eutectic temperature is reached. Then, however, when the osmosis phenomenon stops, the residual amount of intracellular water is sufficient to provoke IIF, so that the abrupt slope change of M_{NaCl}^{int} path reported in Figure 9c takes place at about -35°C. These cells are responsible

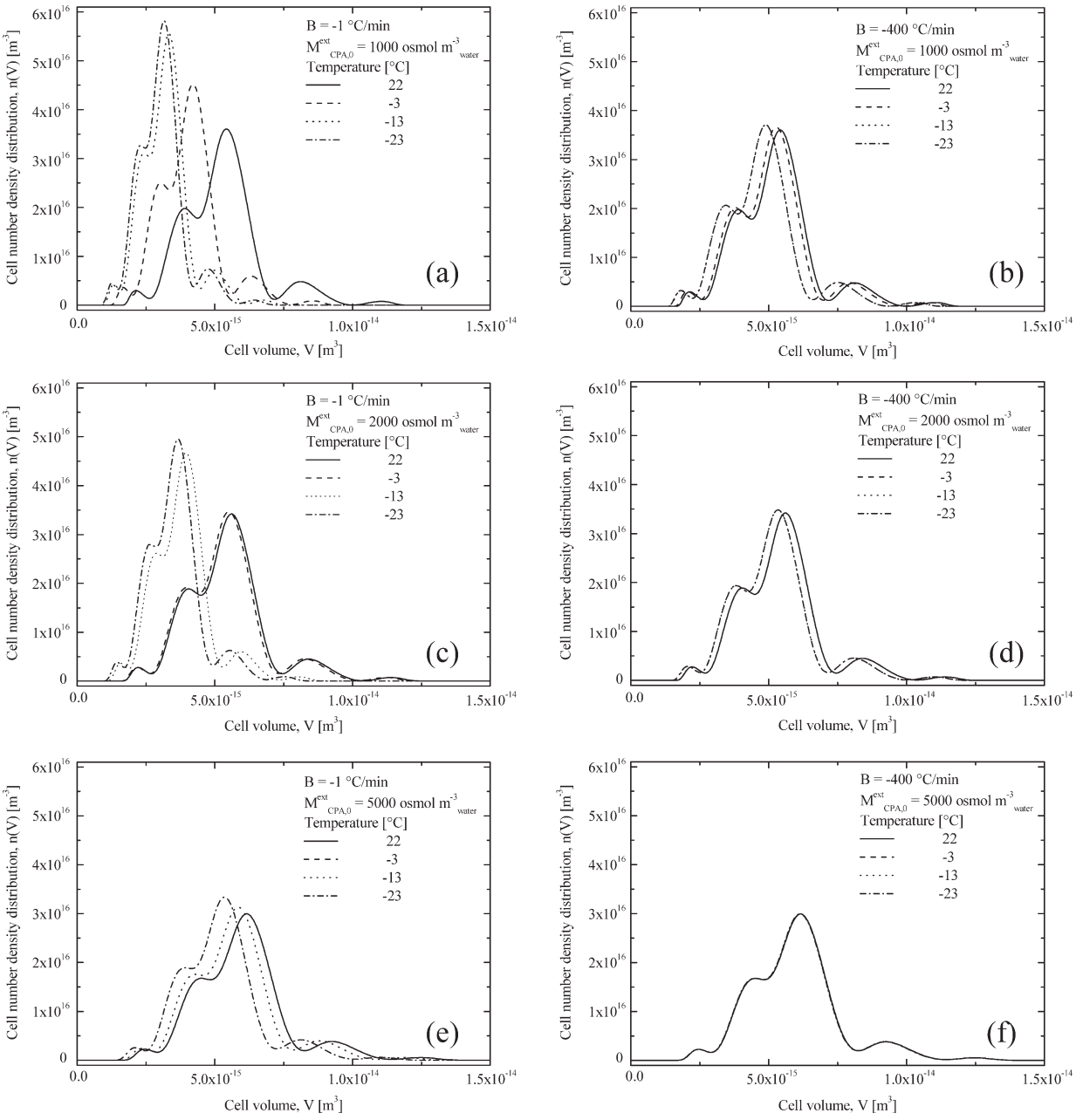

Figure 11. Model results in terms of temporal evolution of the number density distribution of a cell population during cooling at −1 and −400°C min^{-1} at different CPA concentrations.

for the second step of PIIF reported in Figure 9c, where it is seen that a portion of the cell population ices up at about −35°C. However, at this low temperature and high saline concentration, the viscosity of the cytoplasmic solution is so high that ice growth is a relatively slow process, as it may be seen from the difference between PIIF and $PIIF_{init}$ curves reported in Figure 9c. Moreover, due to the significant osmosis, the entrapped and iced up intracellular water volume does not represent a relevant portion of these cells, so that an additional second step for $PIIF_{detect}$ at −35°C is not obtained in Figure 9c. It is worth noting that, working with different cell lineages and operative conditions, Refs. 42, 43 experimentally measured two-step profile of the PIIF vs. temperature plot, similar to the one reported in Figure 9c. It was pointed out that the occurrence of IIF is recognized through darkening or twitching at higher and lower temperatures, respectively. According to Ref. 46, the darkening phenomenon is commonly attributed to Mie scattering by submicron ice crystals (i.e., IIF with large η_{water}), whereas twitching is thought to be associated with nanoscale ice crystals (i.e., IIF with small η_{water}) that are translucent in the visible wavelengths. Therefore, the explanation provided in this work for the two step profile of the PIIF vs. temperature plot seems to be justified. In addition, since according to Ref. 32 the twitching phenomenon cannot be easily detected with the conventional cryomicroscopy technique, the definition of a

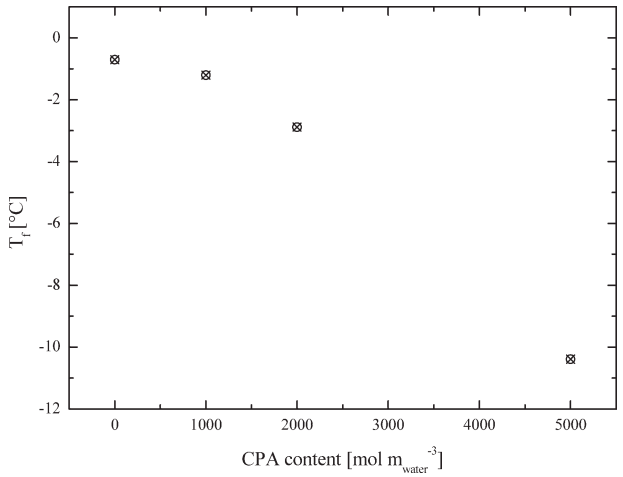

Figure 12. Melting temperature of the ternary system as a function of CPA concentration.

probability of detectable internal ice formation (i.e., $PIIF_{detect}$ in Eq. 48, which does not count the iced up cells with a small amount of internal water content) seems to be appropriate.

In summary, at $-50°C\ min^{-1}$, while for the small cells no IIF occurs down to $-60°C$, both the large and medium size cells form internal ice at temperatures above and below the eutectic one, where a lethal and non-lethal ice volumic content is obtained, correspondingly (see Figure 9d). Therefore, since, according to our model, osmosis may take place only above the eutectic temperature (see Figure 9b), it is apparent that for the large size cells dehydration and IIF occur simultaneously, whereas for the medium size class cells water efflux and ice crystallization take place at different times. This aspect is shown in Figure 9b, where the temporal evolution of the size distribution of the cell population is reported. Indeed, the shift of the size distribution to the left side of the plot during cooling, i.e., toward smaller volumes, is stopped between -3 and $-13°C$ for the largest size classes of the cell population, while it continues for the remaining portion of the size distribution, albeit till the eutectic temperature is reached, as can be noted by comparing Figure 8b with Figure 9b.

The results of the simulations related to $-400°C\ min^{-1}$ are reported in Figure 10. At this relatively high cooling rate, ice is formed inside cells of any size class at temperatures above the eutectic one, in the range -15 to $-5°C$ (Figure 10a). Specifically, IIF takes place first for the large cells (at higher temperatures) and then for the small ones, as clearly depicted by the corresponding abrupt slope change of internal NaCl paths reported in Figure 10a. Water osmosis is relatively slow (Figure 10b) in comparison with ice nucleation and growth, so that PIIF and $PIIF_{init}$ reported in Figure 10c coincide. As a consequence, the relevant amount of entrapped intracellular water ($\eta_{water} > 0.1$) rapidly and completely turns to ice ($\eta_{ice} \rightarrow 1$) for any size class of cells, as shown in Figure 10d. Correspondingly, $PIIF_{detect}$ overlaps to PIIF in Figure 10c. Therefore, in this case, it is likely that the entire population of cells is killed by lethal ice formed at relatively high temperatures. By comparing Figures 8b, 9b, and 10b, it is seen that, during the cooling stage of cryopreservation in absence of CPA, the role played by the osmosis becomes less relevant as cooling rate increases.

When CPA comes into play, the relevance of osmosis phenomenon is further suppressed, as clearly depicted in Figure 11, where the dynamic evolution of the size distribution of the cell population during the cooling stage at the lowest and highest cooling rates considered in this work (i.e., -1 and $-400°C\ min^{-1}$, respectively) are reported for three different glycerol concentrations (i.e., 1000, 2000, and 5000 osmol m^{-3}, respectively). This effect is due to a lower melting temperature of the ternary system water/NaCl/glycerol, when increasing the CPA content [Eq. 19 in Table 1], as shown in Figure 12. When CPA concentration increases, the temporal window for osmosis occurrence (i.e., before reaching the eutectic temperature where it stops) is thus reduced. However, the temperature dependence of membrane permeabilities plays also a role. Ultimately, this is the effect responsible for the paradoxical behavior of the system depicted in Figures 7a, b, where at relatively low cooling rates (namely -1 and $-10°C\ min^{-1}$), IIF occurs at higher temperatures if an increased amount of CPA is used. On the contrary, at relatively higher cooling rates (i.e., $-400°C\ min^{-1}$, Figure 7f), PIIF is inhibited so that it occurs at lower temperatures when increasing CPA content. This result is due to the corresponding higher viscosity and lower diffusivity of the cytoplasmic solution, which is capable to contrast and overcome the limitation of osmosis that would otherwise favor ice nucleation and growth by entrapping more water inside the cells. Of course, at the intermediate cooling rates considered in this work (i.e., -30, -50, and $-100°C\ min^{-1}$, Figures 7c–e), a continuous variation between these two extreme system behaviors is obtained. Indeed, the effects of a reduced time for osmosis or an increased solution viscosity contrast each other until one of them eventually prevails, depending on the CPA content and the size class of the cell population, thus generating the PIIF curve intersection reported in Figure 7e. As a representative example, the case of $-50°C\ min^{-1}$ is addressed in Figure 13. Here, by keeping the cooling rate constant, the system behavior at several, increasing CPA contents (from 0 to 12 kosmol m^{-3}) is analyzed in detail by focusing on the plots of the probabilities of IIF as a function of temperature (left column) and the corresponding distributions of η_{ice} and η_{water} at $-60°C$ reported as functions of the initial cell volume (right column). In the figures reported in the latter one, the initial cell size distribution is also shown to easily discriminate the classes of cells that resulted iced up at $-60°C$ with a significant, lethal amount of intracellular water ($\eta_{ice} \geq 0.5$ and $\eta_{water} \geq 0.1$), from those iced up with a small, innocuous amount of intracellular water ($\eta_{ice} \geq 0.5$ and $\eta_{water} < 0.1$), and the unfrozen ones ($\eta_{ice} < 0.5$); the above classes are indicated by the dark-shaded, light-shaded, or white areas, correspondingly.

It is apparent that, the size distribution may affect the cooling stage of a cell population not only in the absence (Figure 13a, b) but also in the presence of CPA (Figures 13c, d, i, j), respectively. Indeed, differently sized cells may follow different fates. In general, the larger ones are more prone to form a lethal amount of intracellular ice, while the smaller ones may even remain unfrozen and will eventually vitrify. Depending on the specific CPA content and the adopted thresholds of η_{ice} and η_{water}, it may also happen that only a small amount of ice is formed inside medium sized cells (Figure 13d). On the other hand, all the differently

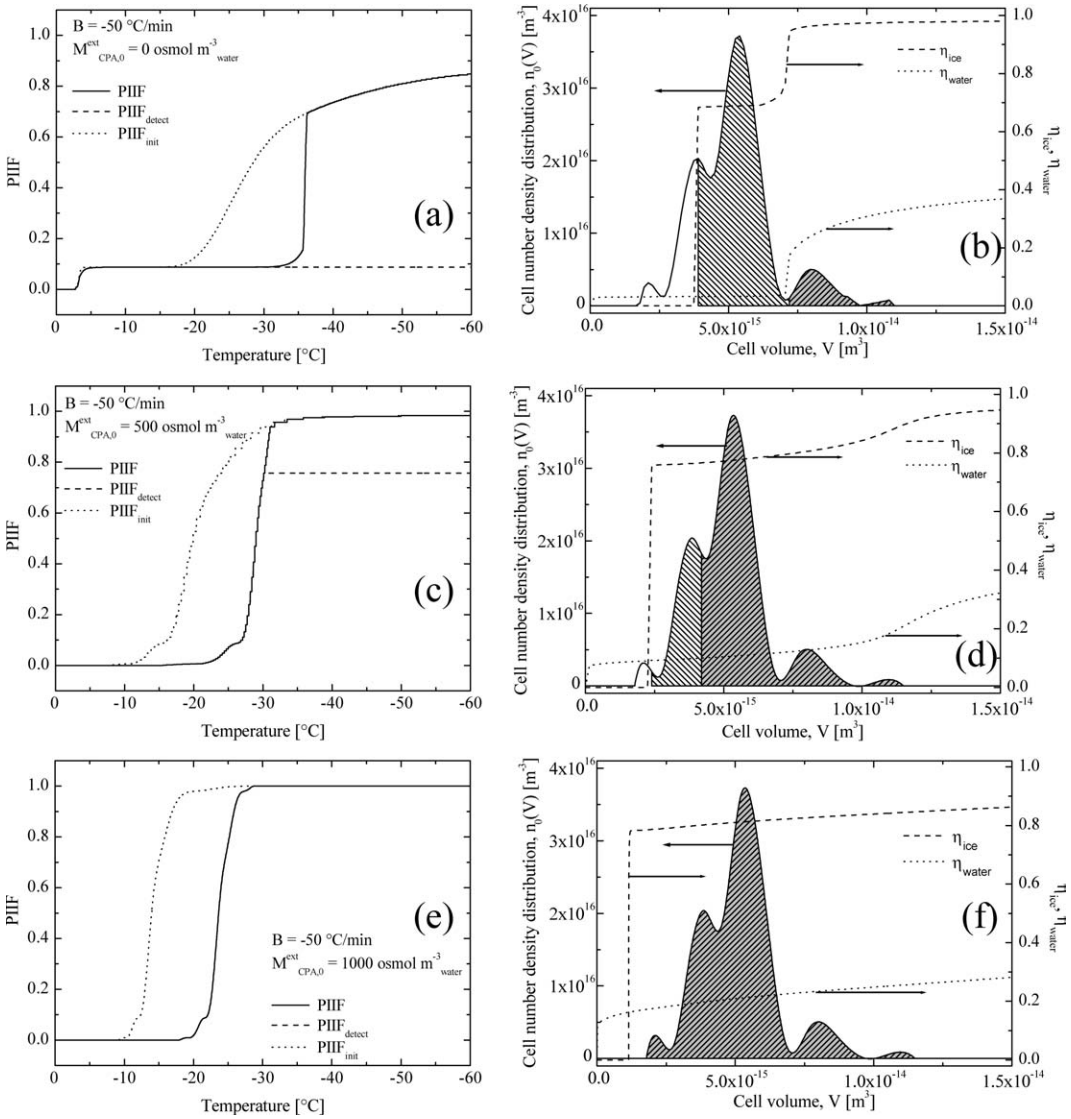

Figure 13. Model results of cooling stage of a cell suspension, carried out at -50°C min^{-1} with increasing CPA content (from 0 to 12 kosmol m^{-3}), in terms of PIIF, $PIIF_{init}$, and $PIIF_{detect}$ (left column plots), and the initial cell size, internal ice volume percentage $\eta_{ice}|_{-60°C}$, and total water content $\eta_{water}|_{-60°C}$ profiles at -60°C as a function of initial cell volume (right column plots).

In right column plots, cells of the initial cell size distribution that are iced up at -60°C with $\eta_{water} \geq 0.1$, $\eta_{water} < 0.1$, or are unfrozen, are indicated by the dark-shaded, light-shaded, or white areas, respectively.

sized cells of the population may behave similarly, as it may be seen from Figures 13f, l, where all size classes result to be lethally iced up at -60°C or unfrozen, correspondingly, even if the temperature of IIF is higher for larger size classes as reported in Figure 13e.

Specifically, by progressively increasing the CPA content, the lethally frozen portion of the cell population indicated by the dark-shaded area initially increases and then decreases, till it completely vanishes, thus showing a maximum. Correspondingly, the PIIF sigmoid reported in the left column plots of Figure 13 first moves toward higher temperatures reaching its maximum value equal to 1 while displaying a more abrupt, sharp variation, and then returns back to the lower ones. Clearly, as discussed previously, the CPA content of 12 kosmol m^{-3} considered in Figure 13k, l may be too high, so that cytotoxicity and excessive volumic range excursions during equilibration stage may not be avoided as mechanisms of cell mortality, even if all the classes of the size distributed cell population will be unfrozen at -60°C and eventually vitrified. However, it is worth noting that, the behavior of IIF shown above, i.e., the occurrence of a maximum value of PIIF, is actually observed at all cooling rates considered in this work. More specifically, to reach a completely unfrozen size distributed cell population at -60°C, a lower CPA content is needed when increasing the cooling rate. Thus, a specific combination of operative conditions (i.e., cooling rate and CPA content) may be found to avoid cytotoxicity and excessive volumic range excursions during equilibration stage, while obtaining a completely unfrozen size distributed cell population at -60°C.

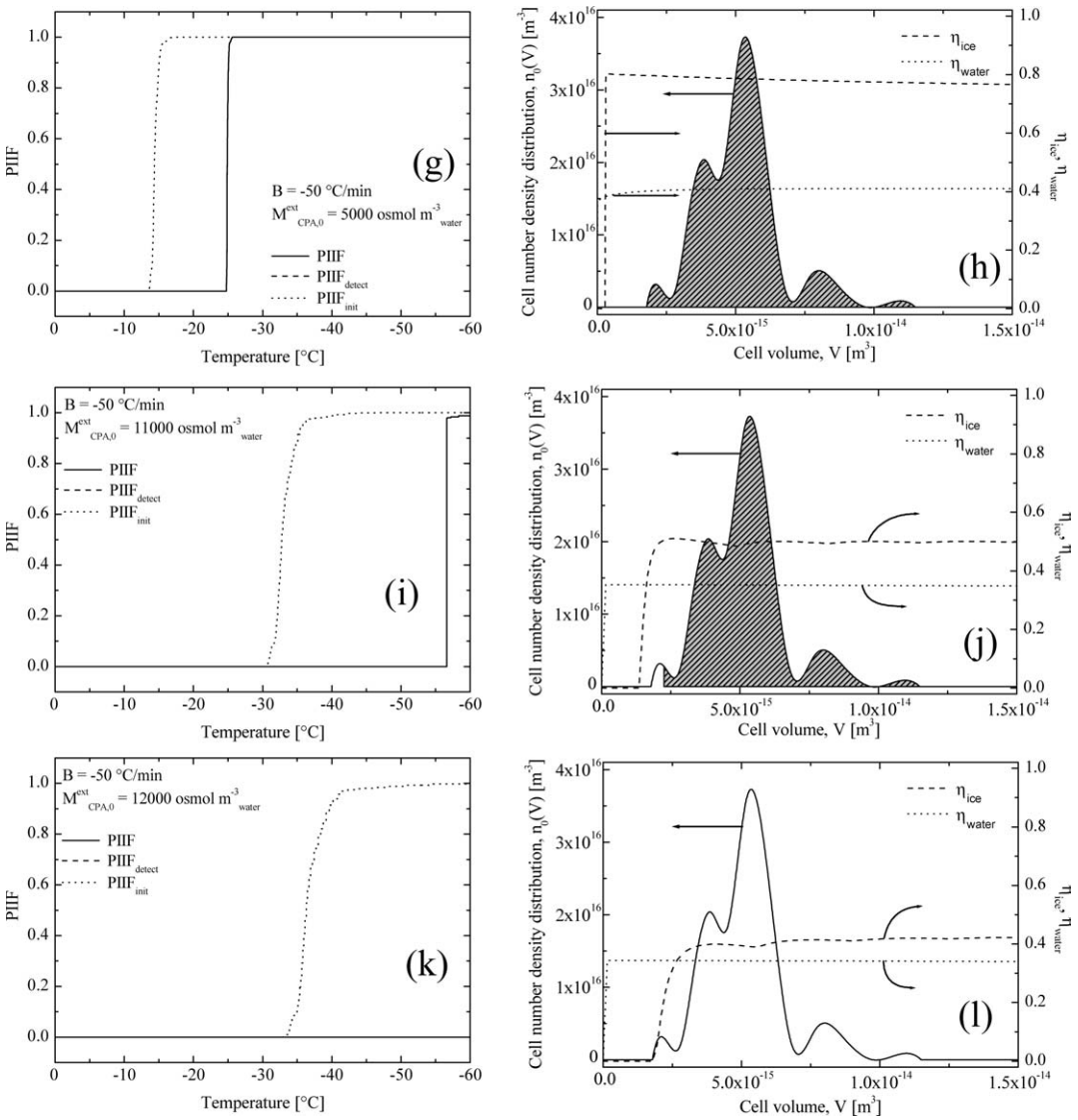

Figure 13. Continued

Basically, the maximum value of PIIF as a function of CPA concentration observed in Figure 13 is the reflection of η_{ice} behavior. Indeed, the η_{ice} profile moves back and forth when increasing CPA content. Thus, IIF starts taking place inside largest class cells and then involves more and more smaller ones up to a certain point at which the opposite behavior occurs. On the contrary, the η_{water} profile keeps moving to the left of the size distribution as CPA content increases. This latter behavior is clearly due to the increasing inhibition of water exo-osmosis, which is progressively limited as CPA content is augmented. The inhibition of osmosis initially favors the IIF by entrapping more iceable water inside the cells, so that η_{ice} profile starts moving toward small volume cells until the CPA content exceeds a certain value, i.e., when intracellular solution viscosity reaches a level that limits IIF and especially the ice crystal growth, as indicated by the increasing gap between PIIF and $PIIF_{init}$ profiles (compare Figure 13g with Figure 13i). At this point, η_{ice} changes its direction toward large volume cells and an increasing portion of the size distribution of the cell population will result unfrozen at -60°C and eventually vitrified, as indicated by the progressive increase of the white area in the right column plots of Figure 13.

Basically, a system behavior at varying CPA content similar to the one reported in Figure 13 for the case of -50°C min^{-1} may be found for the other cooling rates considered in this work. Specifically, at -1°C min^{-1}, a very high CPA concentration needs to be used to obtain a completely unfrozen size distributed cell population at -60°C, while, if CPA is completely absent, an innocuous level of IIF is reached in every size class of the cell population, as reported in Figure 8d. Conversely, at -400°C min^{-1}, a significant, lethal IIF for any cell is obtained without using CPA (Figure 10d), while, with a CPA content as low as 7 kosmol m^{-3}, a completely unfrozen size distributed cell population at -60°C results. Along these lines, high cooling rates need to be combined to high CPA contents for reaching vitrification, while at low cooling rates cell viability may be increased by

adopting relatively low CPA concentrations. These conclusions perfectly match the well known rule of thumb for a successful cryopreservation protocol. Clearly, the values of the operative conditions needed to optimize the process in terms of final cell viability strongly depend on the osmotic characteristics and initial cell size distribution of the specific cell lineage at hand.

Concluding Remarks

In this work, a novel model that is able to quantitatively describe IIF as a function of temperature in a cell population characterized by a size distribution is proposed for the case when a permeant CPA is present. Specifically, the simulation of the initial stage of equilibration (i.e., a one-step CPA permeation kinetics into isotonic rat hepatocytes suspended in a water/NaCl/glycerol solution at ambient temperature), and of the subsequent cooling stage at constant rate down to $-60°C$ is addressed by means of a suitable PBE modeling approach.

The analysis of system behavior (at the several albeit low cooling rates and glycerol concentrations practicable during standard cryopreservation protocols) confirms that, differently sized cells in a single population exhibit different IIF temperatures under the same operative conditions, even in the presence of CPA. Correspondingly, the PIIF results to be related to the initial size distribution of the cell population. In particular, depending on the specific operative conditions adopted, the size distribution and the osmotic properties of the cell lineage at hand, IIF at $-60°C$ may be lethal for a portion of the population (i.e., larger size classes) or it may not reach a dangerous level for the intermediate size class cells, while not even taking place for the smaller ones. Moreover, an original explanation for several, well known experimental evidences, available in a number of articles published in the literature of cell cryopreservation with CPA, is comprehensively given.

Clearly, system behavior during the cryopreservation strongly depends on the osmotic characteristics and initial cell size distribution of the specific cell lineage at hand. Therefore, the proposed model may be effectively used to evaluate the osmotic and IIF parameters of the specific cell lineage under consideration, through direct comparison with suitable experimental data, by properly taking into account the effect of the size distribution. Indeed, to optimize the process in terms of final, post-thaw cell viability, the simulation of the possible homogeneous nucleation at temperatures lower than $-60°C$, as well as the mathematical description of the physico-chemical phenomena taking place during the warming phase need to be addressed. These aspects will be the subjects of our future work.

Acknowledgments

This work was supported by BT (Biomedical Tissues) Srl, Sestu (CA), Italy.

Notation

a_0 = apparent hydrodynamic radius of water molecules in Eq. 35, m
A_t = cell membrane surface area, m^2
$A_{CPA}(M^{int}_{CPA})$ = preexponential factor of the binary water–glycerol solution viscosity, kg m^{-1} s^{-1}
B = constant cooling rate, k s^{-1}
$B_0(t)$ = ice nucleation rate, s^{-1}
c_0 = isotonic salt concentration of cytoplasm, mol m^{-3}
$D(t)$ = water diffusion coefficient in the cytoplasm, m^2 s^{-1}
$\overline{D}(t)$ = average water diffusion coefficient, m^2 s^{-1}
$D_{eq}(t)$ = water diffusion coefficient in the cytoplasm at equilibrium, m^2 s^{-1}
E_{CPA} = apparent activation energy for membrane permeation to CPA, J mol^{-1}
$E_{\eta CPA}$ = activation energy of the binary water–glycerol solution viscosity, kg m^{-1} s^{-1}
E_w = apparent activation energy for membrane permeation to water, J mol^{-1}
E_N = activation energy of nucleation, J
$G_v(V)$ = cell growth rate, m^3 s^{-1}
h = effective number of water molecules in the salt molecule hydration shell
$J(t)$ = ice nucleation rate per unit liquid solution volume, m^{-3} s^{-1}
J_0 = pre-exponential factor of nucleation rate, m^{-4}
k_B = Boltzmann's constant, J K^{-1}
k_e = Einstein's shape factor
$L_p(t)$ = effective membrane permeability to water, m^3 N^{-1} s^{-1}
$L_{p,ref}$ = effective membrane permeability to water at reference temperature T_{ref}, m^3 N^{-1} s^{-1}
$M^{eq,ext}_{CPA}$ (t) = extracellular CPA concentration at equilibrium conditions, [osmol m^{-3}_{water}]
$M^{eq,int}_{CPA}$ (t) = intracellular CPA concentration at equilibrium conditions, osmol m^{-3}_{water}
M^{ext}_{CPA} (t) = extracellular CPA concentration, osmol m^{-3}_{water}
M^{int}_{CPA} (t) = intracellular CPA concentration, osmol m^{-3}_{water}
$M^{ext}_{CPA,0}$ = initial extracellular CPA concentration, osmol m^{-3}_{water}
$M^{eq,ext}_{NaCl}$ (t) = extracellular salt concentration at equilibrium conditions, osmol m^{-3}_{water}
$M^{eq,int}_{NaCl}$ (t) = intracellular salt concentration at equilibrium conditions, osmol m^{-3}_{water}
M^{ext}_{NaCl} (t) = extracellular salt concentration, osmol m^{-3}_{water}
M^{int}_{NaCl} (t) = intracellular salt concentration, osmol m^{-3}_{water}
$M^{ext}_{NaCl,0}$ = initial extracellular salt concentration, osmol m^{-3}_{water}
MW_{CPA} = molecular weight of CPA, g mol^{-1}
MW_{H_2O} = molecular weight of water, g mol^{-1}
MW_{NaCl} = molecular weight of NaCl salt, g mol^{-1}
$n(V,t)$ = cell number density distribution, m^{-3}
$n^0(V)$ = initial cell number density distribution, m^{-3}
$n_{CPA}(t)$ = number of CPA moles inside a cell
n_{NaCl} = number of salt moles inside a cell
$N_{ice}(t)$ = truncated, integer number of ice crystals in a cell
N_{ice} (t) = number of ice crystals in a cell
N^0_{tot} = total number of cells
$P_{CPA}(t)$ = effective membrane permeability to CPA, m s^{-1}
$P_{CPA,ref}$ = effective membrane permeability to CPA at reference temperature T_{ref}, m s^{-1}
$PIIF(t)$ = probability of intracellular ice formation
$PIIF_{detect}(t)$ = probability of detectable intracellular ice formation
$PIIF_{init}(t)$ = probability of initial intracellular ice formation
Q = hydrodynamic interaction constant
$r_i(t)$ = radius of the i-th intracellular ice crystal, m
$r^*(t)$ = critical radius of ice nucleation, m
$\Re$ = universal gas constant, J mol^{-1} K^{-1}
$R(t)$ = mass ratio of CPA to salt, g g^{-1}
$R^{int}(t)$ = intracellular mass ratio of CPA to salt, g g^{-1}
R^{ext} = extracellular mass ratio of CPA to salt, g g^{-1}
S = total solute (NaCl and CPA) mass percentage concentration
$S_{eq}(t)$ = total solute (NaCl and CPA) mass percentage concentration at equilibrium conditions
$S^{ext}_{eq}(t)$ = extracellular total solute (NaCl and CPA) mass percentage concentration at equilibrium conditions
$S^{int}_{eq}(t)$ = intracellular total solute (NaCl and CPA) mass percentage concentration at the equilibrium conditions
t = time, s
t_{eq} = CPA equilibration time, s
t_i = time of i-th intracellular ice crystal formation, s

$T(t)$ = temperature, K
$T_c(M^{int}_{CPA})$ = critical temperature at which the viscosity becomes divergent, K
T_e = eutectic temperature of the binary water–NaCl system, K
T_f = ternary solution fusion temperature, K
T_g (M^{int}_{CPA}) = glass transition temperature, K
T_{init} = initial temperature, K
T_{ref} = reference temperature for determining membrane permeability, K
v_b = osmotically inactive cell volume fraction
v_{CPA} = CPA molar volume, $m^3\ mol^{-1}$
v_{H_2O} = water molar volume, $m^3\ mol^{-1}$
v_{NaCl} = salt molar volume, $m^3\ mol^{-1}$
$V(t)$ = total cell volume, m^3
V_b = osmotically inactive cell volume, m^3
$V_{CPA}(t)$ = intracellular CPA volume, m^3
$V_{ice}(t)$ = intracellular ice volume, m^3
V_{NaCl} = intracellular salt volume, m^3
$V_{water}(t)$ = intracellular liquid water volume, m^3
V_0 = initial, isotonic cell volume, m^3

Greek letters

α = parameter in Eq. 19
β = parameter in Eq. 19
δ = parameter in Eq. 41
γ = surface energy for ice nucleation rate, J m^{-2}
φ = dissociation constant for salt in water
$\phi_s(M^{int}_{NaCl}, M^{int}_{CPA})$ = volume fraction of hydrated salt ions in cytoplasmatic solution
$\eta(t)$ = cytoplasmatic solution viscosity, kg $m^{-1}\ s^{-1}$
$\eta_{ice}(t)$ = intracellular ice volume percentage
$\eta_{CPA}(M^{int}_{CPA}, T)$ = binary water–CPA solution viscosity, kg $m^{-1}\ s^{-1}$
η^{Tg}_{CPA} = binary water–CPA solution viscosity at glass transition temperature, kg $m^{-1}\ s^{-1}$
η^{293K}_{CPA} = binary water–CPA solution viscosity at 20°C, kg $m^{-1}\ s^{-1}$
$\eta_{water}(t)$ = intracellular water volume percentage
σ = reflection coefficient
$\Omega_g(t)$ = ice growth driving force

Literature Cited

1. Karlsson JO, Toner M. *Cryopreservation*. In: Lanza R, Langer R, Vacanti J. editors. *Principles of Tissue Engineering*, 2nd ed. San Diego: Academic press Inc., 2000:293–306.
2. Mazur P, Leibo SP, Chu EH. A two-factor hypothesis of freezing injury. Evidence from Chinese hamster tissue-culture cells. *Exp Cell Res*. 1972;71:345–355.
3. Karlsson JO, Cravalho EG, Toner M. Intracellular ice formation: causes and consequences. *Cryo Letters*. 1993;14:323–336.
4. Mazur P. Freezing of living cells: mechanisms and implications. *Am J Physiol*. 1984;247:C125–C142.
5. Polge C, Smith AU, Parkes AS. Revival of spermatozoa after vitrification and dehydration at low temperatures. *Nature (London)*. 1949; 164:666.
6. Mazur P. Kinetics of water loss from cells at subzero temperatures and likelihood of intracellular freezing. *J Gen Physiol*. 1963;47:347–369.
7. Benson CT, Liu C, Gao DY, Critser ES, Benson JD, Critser JK. Hydraulic conductivity (L_p) and its activation energy (E_a), cryoprotectant agent permeability (P_s) and its E_a, and reflection coefficients (σ) for golden hamster individual pancreatic islet cell membrane. *Cryobiology*. 1998;37:290–299.
8. Woods EJ, Liu J, Gilmore JA, Reid TJ, Gao DY, Crister JK. Determination of human platelet membrane permeability coefficients using the Kedem-Katchalsky formalism: estimates from two- vs three-parameter fits. *Cryobiology*. 1999;38:200–208.
9. Phelps MJ, Liu J, Benson JD, Willoughby CE, Gilmore JA, Critser JK. Effect of Percoll separation, cryoprotective agents, and temperature on plasma membrane permeability characteristics of murine spermatozoa and their relevance to cryopreservation. *Biol Reprod*. 1999;61:1031–1041.
10. Agca Y, Gilmore J, Byers M, Woods EJ, Liu J, Critser JK. Osmotic characteristics of mouse spermatozoa in the presence of extenders and sugars. *Biol Reprod*. 2002;67:1493–1501.
11. Hunt CJ, Armitage SE, Pegg DE. Cryopreservation of umbilical cord blood: 1. Osmotically inactive volume, hydraulic conductivity and permeability of $CD34^+$ cells to dimethyl sulphoxide. *Cryobiology*. 2003;46:61–75.
12. Ebertz SL, McGann LE. Cryoprotectant permeability parameters for cells used in a bioengineered human corneal equivalent and applications for cryopreservation. *Cryobiology*. 2004;49:169–180.
13. Mukherjee IN, Song YC, Sambanis A. Cryoprotectant delivery and removal from murine insulinomas at vitrification-relevant concentrations. *Cryobiology*. 2007;55:10–18.
14. Toner M, Cravalho EG, Karel M. Thermodynamics and kinetics of intracellular ice formation during freezing of biological cells. *J Appl Phys*. 1990;67:1582–1593.
15. Toner M, Tompkins RG, Cravalho EG, Yarmush ML. Transport phenomena during freezing of isolated hepatocytes. *AIChE J*. 1992; 38:1512–1522.
16. Karlsson JO, Cravalho EG, Toner M. A model diffusion-limited ice growth inside biological cells during freezing. *J Appl Phys*. 1994;75: 4442–4445.
17. Zhao G, Luo D, Gao D. Universal model for intracellular ice formation and its growth. *AIChE J*. 2006;52:2596–2606.
18. Karlsson JO. Effect of solution composition on the theoretical prediction of the ice nucleation kinetics and thermodynamics. *Cryobiology*. 2010;60:43–51.
19. Yang G, Zhang A, Xu LX, He X. Modelling the cell-type dependence of diffusion-limited intracellular ice nucleation and growth during both vitrification and slow freezing. *J Appl Phy*. 2009;105: 1147011–11470111.
20. Fadda S, Cincotti A, Cao G. The effect of cell size distribution during the cooling stage of cryopreservation without CPA. *AIChE J*. In press. DOI 10.1002/aic.12137.
21. Bigg EK. The supercooling of water. *Proc Phys Soc B*. 1953;66: 688–694.
22. Zachariassen KE, Kristiansen E, Andre Pedersen S, Hammel HT. Ice nucleation in solutions and freeze-avoiding insects-homogeneous or heterogenous. *Cryobiology*. 2004;48:309–321.
23. Kleinhans FW. Membrane permeability modeling: Kedem-Katchalsky vs a two-parameters formalism. *Cryobiology*. 1998;37:271–289.
24. Elmoazzen HY, Elliott JA, McGann LE. Osmotic transport across cell membranes in nondilute solutions: a new nondilute solute transport equations. *Biophys J*. 2009;96:2559–2571.
25. Rall WF, Mazur P, McGrath JJ. Depression of the ice-nucleation temperature of rapidly cooled mouse embryos by glycerol and dimethyl sulphoxide. *Biophys J*. 1983;41:1–12.
26. Kedem O, Katchalsky A. Thermodynamics analysis of the permeability of biological membranes to non-electrolytes. *Biochim Biophys Acta*. 1958;27:229–246.
27. Levin RL, Cravalho EG, Huggins CE. A membrane model describing the effect of temperature on the water conductivity of erythrocyte membranes at subzero temperatures. *Cryobiol*. 1976;13:415–429.
28. Pegg DE. Simple equations for obtaining melting points and eutectic temperatures for the ternary system glycerol/sodium chloride/water. *Cryo Letters*. 1983;4:259–268.
29. Vand V. Viscosity of solutions and suspensions; theory. *J Phys Colloid Chem*. 1948;52:277–299.
30. Vand V. Viscosity of solutions and suspensions. Experimental determination of the viscosity-concentration function of spherical suspensions. *J Phys Colloid Chem*. 1948;52:300–314.
31. Vand V. Viscosity of solutions and suspensions. Theoretical interpretation of viscosity of sucrose solutions. *J Phys Colloid Chem*. 1948;52:314–321.
32. Stott SL, Karlsson JO. Visualization of intracellular ice formation using high-speed video cryomicroscopy. *Cryobiology*. 2009;58: 84–95.
33. Carnevale KA. Finite-difference model of cell dehydration during cryopreservation. Masters thesis, School of Mechanical Engineering, Georgia Institute of Technology. 2004.
34. Luyet B, Rasmussen D. Study by differential thermal analysis of the temperatures of instability of rapidly cooled solutions of glycerol, ethylene glycol, sucrose and glucose. *Biodynamica*. 1968;10:167–191.

35. Perry RH, Green D. *Perry's Chemical Engineers' Handbook*, 6th ed. New York: McGraw-Hill, 1984.
36. Kresin M, Körber C. Influence of additives on crystallization kinetics: comparison between theory and measurements in aqueous solutions. *J Chem Phys*. 1991;95:5249–5255.
37. Weast RC, editor. *Handbook of chemistry and Physics*, 80th ed. Cleveland: CRC, 1999–2000:8–65.
38. García F, Kierbel A, Larocca MC, Gradilone SA, Splinter P, LaRusso NF, Marinelli RA. The water channel aquaporin-8 is mainly intracellular in rat hepatocytes, and its plasma membrane insertion is stimulated by cyclic AMP. *J Biol Chem.* 2001;276:12147–12152.
39. Fleming KK, Hubel A. Cryopreservation of hematopoietic stem cells: emerging science, technology and issues. *Transfus Med Hemother*. 2007;34:268–275.
40. Hunt CJ, Armitage SE, Pegg DE. Cryopreservation of umbilical cord blood: 2. Tolerance of $CD34^{+}$ cells to multimolar dimethyl sulphoxide and effect of cooling rate on recovery after freezing and thawing. *Cryobiology*. 2003;46:76–87.
41. Karlsson JO, Toner M. Long-term storage of tissues by cryopreservation: critical issues. *Biomaterials*. 1996;17:243–256.
42. Toner M, Cravalho EG, Karel M, Armant DR. Cryomicroscopic analysis of intracellular ice formation during freezing of mouse oocytes without cryoadditives. *Cryobiology*. 1991;28:55–71.
43. Berrada MS, Bischof JC. Evaluation of freezing effects on human microvascular-endothelial cells (HMEC). *Cryo Letters*. 2001;22: 353–366.
44. Aksan A, Toner M. *Roles of thermodynamic state and molecular-mobility in biopreservation*. In: Bronzino JD, editor. *Tissue Engineering and Artificial Organs*. Boca Raton, FL: Taylor & Francis, 2006.
45. Harris CL, Toner M, Hubel A, Cravalho EG, Yarmush ML, Tompkins RG. Cryopreservation of isolated hepatocytes: intracellular ice formation under various chemical and physical conditions. *Cryobiology*. 1991;28:436–444.
46. Scheiwe MW, Körber C. Quantitative cryomicroscopic analysis of intracellular freezing of granulocytes without cryoadditive. *Cryobiology*. 1987;24:473–483.

Manuscript received Feb. 16, 2010, revision received Apr. 30, 2010, and final revision received Jun. 4, 2010.